

Theory of anisotropic elastoresistivity of two-dimensional extremely strongly correlated metals

Michael Arciniaga¹, Peizhi Mai^{2,1}, B Sriram Shastry¹

¹Physics Department, University of California, Santa Cruz, CA 95064, USA and

²Center for Nanophase Materials Sciences, Oak Ridge National Laboratory, Oak Ridge, TN, 37831-6494, USA

(Dated: November 12, 2021)

There is considerable recent interest in the phenomenon of anisotropic electroresistivity of correlated metals. While some interesting work has been done on the iron-based superconducting systems, not much is known for the cuprate materials. Here we study the anisotropy of elastoresistivity for cuprates in the normal state. We present theoretical results for the effect of strain on resistivity, and additionally on the optical weight and local density of states. We use the recently developed extremely strongly correlated Fermi liquid theory in two dimensions, which accounts quantitatively for the unstrained resistivities for three families of single-layer cuprates. The strained hoppings of a tight-binding model are roughly modeled analogously to strained transition metals. The strained resistivity for a two-dimensional t - t' - J model are then obtained, using the equations developed in recent work. Our quantitative predictions for these quantities have the prospect of experimental tests in the near future, for strongly correlated materials such as the hole-doped and electron-doped high- T_c materials.

I. INTRODUCTION & MOTIVATION

Understanding the temperature and doping dependent electrical conductivity of very strongly correlated metals in two dimensions (2D) is a very important problem in condensed matter physics. Recent interest in *elastoresistivity*, i.e., the strain dependence of resistivity has been triggered by the discovery of strong nematicity in iron based superconductors [1–3]. The nematic susceptibility is defined as

$$\chi_{nem} = \lim_{\epsilon_{xx} \rightarrow 0} \frac{\rho'_{xx} - \rho_{xx}}{\rho_{xx}\epsilon_{xx}} \quad (1)$$

where $\rho'_{xx}(\rho_{xx})$ is the x-axis resistivity in presence (absence) of a small strain ϵ_{xx} . The large magnitude of this dimensionless susceptibility ($|\chi_{nem}| \gtrsim 200$), and the peak like features in its temperature dependence suggest enhanced nematic fluctuations in the pnictides.

The situation for cuprates is less studied thus motivating the present work. The recently developed extremely correlated Fermi liquid theory (ECFL) [4] accounts quantitatively for the (unstrained) normal state resistivities of three families of single layer cuprates [6–8]. This theory treats correlation effects within the well-defined t - t' - J model. The model lacks any explicit mechanism to drive large nematic fluctuations, but it is possible that these fluctuations are emergent. It is thus natural to ask if the theory can provide a benchmark scale for elastoresistivity effects in cuprates, as well as to examine if nematic fluctuation are encouraged. Towards this goal we present results for the anisotropic elastoresistivity in various geometries for cuprate materials in the normal state within the extremely correlated Fermi liquid theory (ECFL) [4] as applied to the t - t' - J model for spin- $\frac{1}{2}$ electrons on a

square lattice given by the Hamiltonian

$$H = - \sum_{ij\sigma} t_{ij} \tilde{C}_{i\sigma}^\dagger \tilde{C}_{j\sigma} - \mu \hat{N} + \frac{1}{2} \sum_{ij} J_{ij} \left(\vec{S}_i \cdot \vec{S}_j - \frac{1}{4} n_i n_j \right). \quad (2)$$

Here $t_{ij} = t(t')$ for nearest (next-nearest) neighbour sites ij and is zero otherwise on the square lattice [5], \hat{N} is the number operator, $\tilde{C}_{i\sigma} = P_G C_{i\sigma} P_G$ and P_G is the Gutzwiller projection operator which projects out the doubly occupied states. Also the super-exchange $J_{ij} = J$ when acting on nearest neighbour sites and is zero otherwise. The other symbols have their usual meaning.

While the ECFL theory accounts for the variation of resistivity with a change of hopping parameters, we need another piece of information to calculate elastoresistivity. That is a solution to the independent problem of describing the effects of strain on the hopping parameters of the underlying tight-binding model. In cuprates the t - t' - J model arises as an effective low energy model from downfolding from a three band (or in general multi-band) description obtained within band structure calculations [9–11]. This procedure is not unique since the extent of correlations included in the band structure can differ among different calculations. We take the practical view that the hopping parameters can be chosen to depend parametrically on the distance between atoms, in parallel to the treatment of volume effects in transition metals by V. Heine [12]. Thus in our approach, a small strain can be parametrized through a single variable α relating the hopping to the separation R via the relation

$$t(R) \sim \frac{A}{R^\alpha}. \quad (3)$$

From tight binding theory $\alpha = l_1 + l_2 + 1$, where l_1, l_2 are the angular momenta of the overlapping orbitals [12]. Within this scheme we expect that compression enhances overlap and hence the magnitude of hopping, and conversely stretching reduces overlap. Excluding very strong

multi-band effects we may take $\alpha \in \{2, 5\}$ for cuprates. The single parameter needed for our purpose is α , since A is reabsorbed in the unstrained hopping. We further suggest that one may more realistically estimate this single parameter α by measuring other α dependent variation of physical variables with strain, as described below.

This modeling neglects the possible 3-dimensional effects, where the c-axis propagation could in certain situations influence the 2-dimensional bands indirectly. Also cuprates with many layers per unit cell may have more complex dependence on strain as compared to single layer systems. Despite the above caveats in place, it is still worthwhile to study the model Eq. (2) together with the relation Eq. (3) for understanding the elastoresistivity of single layer cuprates.

The problem of (unstrained) normal state resistivity has been explored in various experiments [13–15] on different materials over last few decades. Experiments reveal interesting and challenging transport regimes, termed the *strange metal* and the *bad metal* regime [16], whose existence is inexplicable within the standard Fermi liquid theory of metals. These results have attracted several numerical studies using the techniques of dynamical mean field theory [17–19], determinant quantum Monte-Carlo method [20,21] and dynamical cluster approximation [22,23] etc. These studies indicate that the unusual regimes are indicative of very strong correlations of the Mott-Hubbard variety.

Despite the numerical progress, few analytical techniques are available to extract the low temperature transport behavior, and thus better understand the various regimes. This is due to the inherent difficulties of treating strong correlations, i.e., physics beyond the scope of perturbation theory. Recently, the extremely correlated Fermi liquid theory (ECFL) [4,24,25] has been developed by Shastry and coworkers. This theory consists of a basic reformulation of strong correlation physics, and its many applications have been reported for the t - t' - J model in dimensions $d=1,2,\infty$. This is a minimal and fundamental model to describe extreme correlations. The ECFL theory leads to encouraging results which are in close accord with experiments such as spectral line shape in angle-resolved photoemission spectroscopy (ARPES) [7,8,26–31], Raman susceptibility [32,33], and particularly, resistivity [7,8,25,34]. A recent work [6] shows that the ECFL theory gives a quantitatively consistent account of the T and density dependence of the resistivity for single layer hole-doped and electron-doped correlated materials. Here we explore the strain dependence of the resistivity within the same scheme.

In the ECFL theory, the resistivity arises from (umklapp-type) inelastic scattering between strongly correlated electrons. Here the hopping amplitudes of electrons play a dual role. The first one, that of propagating the fragile quasiparticles, is standard in all electronic systems. They provide a simple model for the band structure. Additionally, for very strong correlations the ECFL theory shows that the hopping parameters are

also involved in the scattering of quasiparticles off each other [35]. A surprisingly low characteristic temperature scale [8,34] emerges from the strong correlations, above which the resistivity crosses over from Fermi liquid type i.e. $\rho \sim T^2$ behavior, to an almost linear type i.e. $\rho \sim T$ behavior [7,8,15].

From the above we argue that strain effects could provide a test of the underlying mechanism for resistivity within the ECFL theory to include strain dependence. Experiments probing these strain effects are likely in the near future, thus enabling an important test of the theory. For the purpose of independently estimating the strain-hopping parameter α in Eq. (3), we have identified two experimentally accessible variables. Firstly we study the integrated weight of the anisotropic electrical optical conductivity, i.e., the f-sum rule weight, accessible in optical experiments [36,37]. Secondly we study the local density of states (LDOS), measurable through scanning tunneling microscopy (STM) [38–42]. The f-sum rule weight in tight binding systems is related to the expectation of the kinetic energy, or hopping, and can be obtained from the Green's function. The LDOS can also be calculated from the local Green's function easily.

The plan of the paper is as follows: In Sec. II (A) we introduce the t - t' - J model and summarize the second order ECFL equations and the corresponding Green's functions and self-energies. (B) We describe how to convert the lattice constants and hopping parameters for a system under strain. (C) We outline the parameters for the program. In Sec. III, we present the detailed calculation for and results of (A) the resistivity, (B) the kinetic energy, and (C) the LDOS and their associated susceptibilities with respect to strain. We provide a brief summary and discussion of our results and future work in Sec. IV.

II. METHODS & PARAMETERS

A. The Model

It has been argued that the t - t' - J model is key to describing the physics of high- T_c superconducting materials [43]. This model is composed of two terms: $H_{tJ} = H_t + H_J$ where H_t is derived by taking the infinite- U limit of the Hubbard model plus an additional term H_J which introduces antiferromagnetic coupling. The general Hamiltonian Eq. (2) can be rewritten in terms of the Hubbard X operators [4] as

$$\begin{aligned} H_t &= - \sum_{ij\sigma} t_{ij} X_i^{\sigma 0} X_j^{0\sigma} - \mu \sum_{i\sigma} X_i^{\sigma\sigma}, \\ H_J &= \frac{1}{2} \sum_{ij\sigma} J_{ij} X_i^{\sigma\sigma} \\ &\quad + \frac{1}{4} \sum_{ij\sigma_1\sigma_2} J_{ij} \{ X_i^{\sigma_1\sigma_2} X_j^{\sigma_2\sigma_1} - X_i^{\sigma_1\sigma_1} X_j^{\sigma_2\sigma_2} \} \end{aligned} \quad (4)$$

Here t_{ij} and J_{ij} are already defined below Eq. (2). We present results for both vanishing and non-vanishing J_{ij} . The operator $X_i^{ab} = |a\rangle\langle b|$ takes the electron at site i from the state $|b\rangle$ to the state $|a\rangle$ where $|a\rangle$ and $|b\rangle$ are one of the three allowed states: two occupied states $|\uparrow\rangle, |\downarrow\rangle$, or the unoccupied state $|0\rangle$ — the appropriate X operator referring to the doubly occupied state $|\uparrow\downarrow\rangle$ is excluded in both the Hamiltonian and state space. The X operator relates to the alternative representation used in Eq. 2 as follows: $X_i^{\sigma 0} \rightarrow \tilde{C}_{i\sigma}^\dagger$, $X_i^{\sigma 0} \rightarrow \tilde{C}_{i\sigma}$ and $\sum_\sigma X_i^{\sigma\sigma} \rightarrow n_i$.

B. The ECFL Equations

In this section, we briefly introduce the ECFL equations for the t - t' - J model. More details can be found in Ref. [4,7,24,25]. In the ECFL theory, the one-electron Green's function \mathcal{G} is found using the Schwinger method [44] and in momentum space is factored as a product of an auxiliary Green's function \mathbf{g} and a “comparison” function $\tilde{\mu}$:

$$\mathcal{G}(k) = \mathbf{g}(k) \times \tilde{\mu}(k) \quad (5)$$

where $k \equiv (\vec{k}, i\omega_k)$, and $\omega_k = (2k+1)\pi k_B T$ is the Fermionic Matsubara frequency and subscript k is an integer. The auxiliary $\mathbf{g}(k)$ plays the role of a Fermi-liquid type Green's function whose asymptotic behavior is $1/\omega$ as $\omega \rightarrow \infty$, and $\tilde{\mu}$ is an adaptive spectral weight that mediates between two conflicting requirements [24]: (1) the high frequency behavior of the non-canonical fermions and (2) the Luttinger-Ward volume theorem at low frequencies.

The Schwinger equation of motion for the physical Green's function can be symbolically written as [24]

$$(\mathbf{g}_0^{-1} - \hat{X} - Y_1) \cdot \mathcal{G} = \delta (1 - \gamma). \quad (6)$$

where \hat{X} represents a functional derivative and Y_1 describes a Hartree-type energy, i.e., \mathcal{G} convoluted with hopping and exchange interactions. The left hand side of Eq. (6) is analogous to that of the Schwinger-Dyson equation for Hubbard model [45]: $(\mathbf{g}_0^{-1} - U\delta/\delta\mathcal{V} - U\mathcal{G}) \cdot \mathcal{G} = \delta \mathbf{1}$. Observe on the right side of Eq. (6), the essential difference is the γ term which is proportional to a local \mathcal{G} and originates from the non-canonical algebra of creation and annihilation operators. The non-canonical nature of operators and the lack of an obvious small parameter for expansion present the main difficulties towards solving this equation.

To tackle these difficulties, the ECFL theory inserts into Eq. (6) the λ parameter

$$(\mathbf{g}_0^{-1} - \lambda\hat{X} - \lambda Y_1) \cdot \mathcal{G} = \delta (1 - \lambda\gamma). \quad (7)$$

where $\lambda \in [0, 1]$ interpolates from a non-interacting to fully interacting system. This parameter plays a parallel role to that of inverse spin parameter $1/2S$ in quantum

magnets, where S is the magnitude of the spin. Then we expand Eq. (7) systematically with respect to λ up to a finite order and at the end set $\lambda = 1$ to recover the full t - t' - J physics. The introduction of λ bound to $[0, 1]$ in ECFL makes it possible that a low-order expansion could be enough to describe low-energy excitations in a large region of doping. This argument has been justified in one [46] and infinite [25] dimensions by benchmarking against exact numerical techniques and in two [7,8] dimensions by comparing well with experiments.

In the following, we use the minimal version of second order (in λ) ECFL equations [7]:

$$\tilde{\mu}(k) = 1 - \lambda \frac{n}{2} + \lambda \psi(k) \quad (8)$$

$$\mathbf{g}^{-1}(k) = i\omega_k + \boldsymbol{\mu} - \epsilon_{\vec{k}} + \lambda \frac{n}{2} \epsilon_{\vec{k}} - \lambda \phi(k) \quad (9)$$

where $\boldsymbol{\mu}$ is the chemical potential (denoted in bold-face) and $\epsilon_{\vec{k}}$ is the bare band energy found by taking the Fourier transformation of the hopping parameter. The physical Green's function features two self-energy terms: the usual Dyson-like self-energy denoted $\phi(k)$ in the denominator and a second self-energy in the numerator $\psi(k)$. The self-energy $\phi(k)$ can conveniently be decomposed as follows: $\phi(k) = \chi(k) + \epsilon'_{\vec{k}} \psi(k)$ where $\chi(k)$ denotes a self-energy part, $\epsilon'_{\vec{k}} = \epsilon_{\vec{k}} - u_0/2$ and $\psi(k)$ the second self-energy. Here u_0 acts as a Lagrange multiplier, enforcing the shift invariance [4,7,24] of the t - t' - J model at every order of λ . The two self-energies functions ψ and χ expanded formally in λ to second order approximation $\mathcal{O}(\lambda^2)$ are $\psi = \psi_{[0]} + \lambda\psi_{[1]} + \dots$ and $\chi = \chi_{[0]} + \lambda\chi_{[1]} + \dots$. The expression for these self-energies in the expansion are

$$\psi_{[0]}(k) = 0, \quad \chi_{[0]}(k) = - \sum_p \left(\epsilon'_{\vec{p}} + \frac{1}{2} J_{\vec{k}-\vec{p}} \right) \mathbf{g}(p) \quad (10)$$

and

$$\psi_{[1]}(k) = - \sum_{pq} \left(\epsilon'_{\vec{p}} + \epsilon'_{\vec{q}} + J_{\vec{k}-\vec{p}} \right) \mathbf{g}(p) \mathbf{g}(q) \mathbf{g}(p+q-k) \quad (11)$$

$$\begin{aligned} \chi_{[1]}(k) = & - \sum_{pq} \left(\epsilon'_{\vec{p}} + \epsilon'_{\vec{q}} + J_{\vec{k}-\vec{q}} \right) \left(\epsilon'_{\vec{p}+\vec{q}-\vec{k}} + J_{\vec{k}-\vec{p}} \right) \\ & \times \mathbf{g}(p) \mathbf{g}(q) \mathbf{g}(p+q-k) \end{aligned} \quad (12)$$

where $\sum_k \equiv \frac{k_B T}{N_s} \sum_{\vec{k}, \omega_k}$ and $J_{\vec{q}}$ is the Fourier transform of J_{ij} [47]. By setting λ to 1, the resulting expressions for the ECFL equations expanded to $\mathcal{O}(\lambda^2)$ are

$$\tilde{\mu}(k) = 1 - \frac{n}{2} + \psi(k) \quad (13)$$

$$\begin{aligned} \mathbf{g}^{-1}(k) = & i\omega_k + \boldsymbol{\mu} - \epsilon_{\vec{k}} + \frac{n}{2} \epsilon_{\vec{k}} - \chi_{[0]}(k) \\ & - \chi_{[1]}(k) - \epsilon'_{\vec{p}} \psi_{[1]}(k) \end{aligned} \quad (14)$$

We can verify that an arbitrary shift of $\epsilon_{\vec{k}} \rightarrow \epsilon_{\vec{k}} + \mathbf{c}_0$ leaves the above expression invariant by shifting $\boldsymbol{\mu} \rightarrow$

$\mu + \mathbf{c}_0$ and $u_0 \rightarrow u_0 + 2\mathbf{c}_0$. In this sense, we may take u_0 as a second chemical potential. We can determine the two chemical potentials μ and u_0 by satisfying the following number sum rules

$$\sum_k \mathbf{g}(k) e^{i\omega_k 0^+} = \frac{n}{2} = \sum_k \mathcal{G}(k) e^{i\omega_k 0^+}, \quad (15)$$

where n is the particle density. We find the spectral function $\rho_{\mathcal{G}}(k) = -1/\pi \Im m \mathcal{G}(k)$ by analytically continuing (i.e. $i\omega_k \rightarrow \omega + i\eta$) and by solving Eq. (5) and Eqs. (10-15) iteratively. We remind the reader that the spectral function $\rho_{\mathcal{G}}(\vec{k}, \omega)$ is referred to in most experimental literature by the symbol $A(\vec{k}, \omega)$. We can recover the interacting Green's function from $\rho_{\mathcal{G}}$ using

$$\mathcal{G}(\vec{k}, i\omega_k) = \int_{-\infty}^{\infty} \frac{\rho_{\mathcal{G}}(\vec{k}, \nu)}{i\omega_k - \nu} d\nu. \quad (16)$$

C. Strain effects on hopping and exchange

§Converting lattice constant changes to hopping changes: The t-t'-J model in two dimensions describes the hopping of electrons between copper atoms in the 2-d plane. In this model, the hopping parameters with strain and without strain are denoted as

$$\{t_x, t_y, t_d\} \rightarrow \{t, t, t'\}. \quad (17)$$

Thus under strain t_x and t_y refer to nearest neighbor hops along x and y axes, and t_d is the second neighbor hopping along the diagonal of the square lattice. We start with the tetragonal symmetry case $t_x = t_y = t$ where there are just two parameters t, t' .

At the level of a single bond between two coppers, any generic hopping $t(R)$ for a bond with length R can be represented by [12]

$$t(R) \sim \frac{A}{R^\alpha} \quad (18)$$

where A is a constant. In the simplest cases, the exponent α is given by the angular momentum l_1, l_2 of the relevant atomic shells of the two atoms by the formula

$$\alpha = l_1 + l_2 + 1. \quad (19)$$

Thus for two copper atoms $l_1 = l_2 = 2$ and hence we might expect

$$\alpha \sim 5, \quad (20)$$

whereas for copper oxygen bonds $l_1 = 2, l_2 = 1$, therefore

$$\alpha \sim 3. \quad (21)$$

For the effective single band description of the cuprate materials, it is not entirely clear what value of α is most appropriate. Comparisons with experiments might be

the best way to decide on this question, when the results become available. Until then we can bypass this issue by presenting the theoretical results in terms of $\frac{\delta t}{t}$ rather than the strain itself. Towards this end Eq. (18) is a very useful result. We rewrite it as

$$\frac{\delta t(R)}{t(R)} = -\alpha \frac{\delta R}{R}, \quad (22)$$

thus enabling us to convert a change of the lattice constant to that of the corresponding hopping, using only the value of t and α . Throughout this paper we will refer to $\delta t/t$ as “strain” or with emphasis as “hopping strain” in order to distinguish it from “conventional strain” $\delta R/R$. Strain will always refer to variations along the x -axis unless otherwise noted.

§Geometrical aspects of the strain variation

Our calculation studies a few variations of parameters. We start on a lattice with tetragonal symmetry at $t \sim 5220\text{K}$ (0.45eV), and we vary t' to capture both electron-doped ($t' > 0$) and hole-doped ($t' < 0$) cuprates. The magnitude of t is only a crude estimate, it is refined for different single layer cuprate systems in Ref. [6].

On the distorted lattice with orthorhombic symmetry and lattice constants a and b , the three distances of interest (two sets of nearest neighbors and one set of second neighbors) are

$$a, b, \rho = \sqrt{a^2 + b^2}. \quad (23)$$

For the tetragonal case we refer to the undistorted lattice parameter as a_0 , thus $a = b = a_0, \rho = \sqrt{2}a_0$. We next study the effect of stretching ($\delta a > 0$) or compressing ($\delta a < 0$) the x -axis lattice constant, leaving the y -axis unchanged. The changes in the lattice constants then read as

$$a \rightarrow a_0 + \delta a; \quad b \rightarrow a_0; \quad \rho \rightarrow \sqrt{2}a_0 + \frac{\delta a}{\sqrt{2}}. \quad (24)$$

We denote the strain in the x -direction as

$$\epsilon_{xx} = \frac{\delta a}{a_0}. \quad (25)$$

In terms of the strain, we can rewrite the distances to neighbors as

$$a = a_0(1 + \epsilon_{xx}), \quad b = a_0, \quad \rho = \sqrt{2}a_0 \left(1 + \frac{\epsilon_{xx}}{2}\right), \quad (26)$$

so that $\epsilon_{xx} > 0$ is regarded as stretching and $\epsilon_{xx} < 0$ as compression. The single particle (tight-binding) energies for the distorted lattice are given by

$$\epsilon_{\vec{k}} = -2t_x \cos(k_x a) - 2t_y \cos(k_y b) - 4t_d \cos(k_x a) \cos(k_y b).$$

In terms of the band parameters of the unstrained system t and t' , we can write the anisotropic band parameters as

$$t_x = (1 - \alpha \epsilon_{xx}) t, \quad t_y = t, \quad t_d = \left(1 - \alpha \frac{\epsilon_{xx}}{2}\right) t', \quad (27)$$

where the factor of $\frac{1}{2}$ for t_d comes about due to a shorter stretching of ρ as in Eq. (26). Their strain variations are denoted by

$$\frac{\delta t_x}{t_x} \equiv \frac{\delta t}{t} = -\alpha \epsilon_{xx}, \quad \frac{\delta t_y}{t_y} = 0, \quad \frac{\delta t_d}{t_d} = -\frac{1}{2} \alpha \epsilon_{xx}. \quad (28)$$

These formulas relate the change in hopping to the physical strain, and thus involve the parameter α which is somewhat uncertain. For that reason, we actually vary $\frac{\delta t}{t}$ in this study. We also go beyond the linear response regime, i.e., we use larger values of $\frac{\delta t}{t}$ than those attainable in the laboratory. In such a case we set $\frac{\delta t_d}{t_d} = \frac{\delta t}{2t}$. To summarize the sign convention used in this work,

$$\begin{aligned} \text{compress: } & \frac{\delta t}{t} > 0, \quad \epsilon_{xx} < 0 \\ \text{stretch: } & \frac{\delta t}{t} < 0, \quad \epsilon_{xx} > 0. \end{aligned} \quad (29)$$

§Converting hopping changes into exchange changes: In this model, the super-exchange interaction maps to hopping as follows: $J = t^2/U$ where U is the on site energy of the Hubbard model. As we vary the hopping parameter, we find $\delta J = 2(\delta t/t)J$ since U does not vary with strain. In this model the first neighbor exchange parameters with and without strain, similar to Eq. 17, are denoted as

$$\{J_x, J_y\} \rightarrow \{J, J\}, \quad (30)$$

where J_x and J_y refer to the first neighbor exchange interactions along the x and y axes. In terms of hopping changes we can rewrite the exchange parameters as

$$J_x = \left(1 + 2\frac{\delta t_{xx}}{t_{xx}}\right) J, \quad J_y = J. \quad (31)$$

D. Parameters in the program

The model considered applies to several classes of materials, such as the cuprates, the sodium cobaltates, and presumably also to the iron arsenide superconductors. We shall restrict our discussion to the cuprates where the parameters are fairly well agreed upon in the community [6,43,48].

In this calculation, we set $t = 1$ as our energy scale and we allow t'/t to vary between -0.4 and 0.4 , to cover the full range of cuprate materials. The hopping strain $\delta t/t$ is varied from -0.15 to 0.15 . The exchange parameter J is set to zero except where otherwise noted. We convert the energy to physical units by setting $t = 0.45\text{eV}$, and hence the bandwidth is $W = 8t = 3.6\text{eV}$. If one wants to make a different choice for t , this can be done by rescaling the energies and T 's by the same scaling factor.

We focus on the optimal doping case $\delta = 0.15$ for cuprate materials [49]. Here δ refers to the hole doping

and relates to the particle density as follows $\delta \equiv (1 - n)$. The temperature range is set to $T \in [37, 450]\text{K}$. Lower temperatures than this lie outside the range of convergence for the current scheme. For the interacting system we solve the ECFL equations (10-15) iteratively on a real frequency grid of size $N_\omega = 2^{14}$ within the range $[-2.5W, 2.5W]$, where W is the bare bandwidth, and a lattice $L \times L$ with $L = 61, 79, 135$. The scale of the frequency grid is tuned to capture the low- T physics. A frequency grid of size $N_\omega = 2^{16}$ only slightly improves our results at much larger computational costs. We primarily use an $L > 61$ for $t' > 0$ at low temperatures (i.e., $T < 100\text{K}$) in order to get sufficient resolution to converge electrical resistivity calculation. The need for a high resolution lattice at low temperatures is a product of the spectral function which features higher, sharper peaks for $t' > 0$, to which the resistivity calculation is sensitive [7], i.e., a larger grid is required to settle the unphysical oscillations in the resistivity calculation. For the non-interacting system we compute LDOS using a system of size $N_\omega = 2^{12}$ and $L = 271$.

III. RESULTS

Here we present the effects of strain along the x-axis on electrical resistivity, kinetic energy and LDOS and their associated susceptibilities in response to a compressive ($\delta t/t > 0$) and tensile ($\delta t/t < 0$) hopping strain.

A. Resistivity for an x-axis strain:

We now study the response of electrical resistivity ρ_α characterized by electron-electron scattering [7] in the presence of a strain. We use the bubble approximation, factoring the current correlator as $\langle J(t)J(0) \rangle \sim \sum_k v_k^2 \mathcal{G}^2(k)$ with suitable vertices v_k and dressed Green's function \mathcal{G} , to compute the conductivity σ_α . Our picture of a quasi-2D metal consists of well separated Cu-O planes and hence each plane can be characterized using the 2D t - J model. The weak k -dependence of the self-energy as seen in Fig. 3 of Ref. [8] diminishes the significance of vertex corrections. In fact the self-energy is completely k -independent in the $d=\infty$ limit and studies in this limit [34] have successfully implemented the bubble approximation while completely ignoring vertex corrections. We shall calculate and quote the following objects denoting the irreducible representations of the D_{4h} point group by the standard names [2,50-52]

- $\rho'_{xx}(T)$ the strained version of resistivity along x-axis.
- $\rho'_{yy}(T)$ the strained version of resistivity along y-axis.
- ρ_{xx} without a prime refers to the tetragonal result, which is the same as ρ_{yy} .

- XX component variations:

$$-(\rho'_{xx} - \rho_{xx})/(\rho_{xx}\delta t/t) \text{ vs } T$$

- YY component variations:

$$-(\rho'_{yy} - \rho_{yy})/(\rho_{yy}\delta t/t) \text{ vs } T$$

- A_{1g} symmetry variations:

$$-\frac{\rho'_{xx} + \rho'_{yy} - 2\rho_{xx}}{2\rho_{xx}\delta t/t} \text{ vs } T$$

- B_{1g} symmetry variations:

$$-\frac{\rho'_{xx} - \rho'_{yy}}{\rho_{xx}\delta t/t} \text{ vs } T$$

Of special interest are the $\rho'_{xx} + \rho'_{yy}$ response which corresponds to the A_{1g} irreducible representation (irrep) and $\rho'_{xx} - \rho'_{yy}$ response, corresponding to the B_{1g} irrep.

§Computation of the anisotropic resistivity

To find the anisotropic resistivity, we compute the dimensionless conductivity [7] for the anisotropic case

$$\sigma_{xx} = \langle \Upsilon_{\vec{k}} (\hbar v_{\vec{k}}^x)^2 / (ab) \rangle_k, \quad (32)$$

$$\sigma_{yy} = \langle \Upsilon_{\vec{k}} (\hbar v_{\vec{k}}^y)^2 / (ab) \rangle_k \quad (33)$$

where $\langle A \rangle_k = \frac{1}{N_s} \sum_{\vec{k}} A$, $N_s = L \times L$ and

$$\Upsilon_{\vec{k}} = (2\pi)^2 \int_{-\infty}^{\infty} d\omega (-\partial f / \partial \omega) \rho_G^2(\vec{k}, \omega) \quad (34)$$

where $f(\omega) \equiv 1/(1 + \exp(\beta\omega))$ is the Fermi function, $\rho_G(k)$ is the spectral function from ECFL theory up to $\mathcal{O}(\lambda^2)$, and $v_{\vec{k}}^x, v_{\vec{k}}^y$ are the bare vertices, which are defined as

$$v_{\vec{k}}^x = \frac{1}{\hbar} \frac{\partial \epsilon_{\vec{k}}}{\partial k_x} = \frac{a}{\hbar} \frac{\partial \epsilon_{\vec{k}}}{\partial k_1}, \quad (35)$$

$$v_{\vec{k}}^y = \frac{1}{\hbar} \frac{\partial \epsilon_{\vec{k}}}{\partial k_y} = \frac{b}{\hbar} \frac{\partial \epsilon_{\vec{k}}}{\partial k_2} \quad (36)$$

where $k_1 = k_x a$ and $k_2 = k_y b$ denote the components of the dimensionless momenta. Inserting the dimensionless momenta into Eq. (33), we obtain

$$\sigma_{xx} = \left\langle \Upsilon_{\vec{k}} \left(\frac{d\epsilon_{\vec{k}}}{dk_1} \right)^2 (a/b) \right\rangle_k, \quad (37)$$

$$\sigma_{yy} = \left\langle \Upsilon_{\vec{k}} \left(\frac{d\epsilon_{\vec{k}}}{dk_2} \right)^2 (b/a) \right\rangle_k \quad (38)$$

for the dimensionless conductivity. The corresponding dimensionless resistivities are $\rho_{xx} = 1/\sigma_{xx}$ and $\rho_{yy} = 1/\sigma_{yy}$.

The electrical resistivity can be converted to physical units as follows: $\rho_{\text{physical}, \alpha} = \rho_{\alpha} \times \rho_0$ where $\rho_0 = c_0 \hbar / e^2 (\sim 1.171 \text{ m}\Omega\text{cm})$ sets the scale for the resistivity,

and $\alpha = xx$ describes the longitudinal (i.e., current $\parallel \epsilon_{xx}$) resistivity and yy describes the transverse (i.e., current $\perp \epsilon_{xx}$) resistivity. Here $c_0 \sim 6.645 \text{ \AA}$ is the typical separation between parallel Cu-O planes [6,53]. In order to estimate the magnitude of the inelastic scattering, we can relate the dimensionless resistivity to $\langle k_F \rangle \ell$ as follows $\langle k_F \rangle \ell = 1/\rho_{\alpha}$ as argued in Refs. [15,54] for quasi-2D materials, where $\langle k_F \rangle$ is an (angle averaged) effective Fermi momentum and ℓ is the mean-free-path. Hence we expect $\rho_{\alpha}/\rho_0 < 1$ in a good metal.

1. The raw resistivities

We first present the effects of hopping strain $\delta t/t$ on resistivity. In Fig. 1, we study the anisotropy of the raw dimensionless resistivity over a broad range of temperatures at the optimal density $n = 0.85$. Fig. 1 displays the longitudinal resistivity ρ_{xx} (solid) and the transverse resistivity ρ_{yy} (dashed) for a compressive strain (red) and tensile strain (blue) in comparison to the unstrained tetragonal system (green). Here we used a representative magnitude of compressive strain $\delta t/t = 0.10$ (i.e. $\epsilon_{xx} \sim -0.02$). We observe that longitudinal resistivity under a compressive strain ($\delta t/t > 0$) is reduced, and conversely, under a tensile strain ($\delta t/t < 0$) it is enhanced across the displayed temperature range for all t' . The response for transverse resistivity is less than the longitudinal one in magnitude. An interesting new feature lies in the t' dependence, we note that magnitude and sign of the change in transverse resistivity is controlled by t' , e.g., for $t' = 0.2t$ the resistivity is almost unchanged for all strains.

These behaviors can be understood qualitatively in the following ways. First, let us look at the simplest case with $t' = 0$ as in Fig. 1 panel (c). When the system is compressed in the x-axis, the hopping t_x rises according to Eq. (27) and so does the conductivity along the same direction, and vice versa. Hence, the longitudinal resistivity gets suppressed (enhanced) under compressive (tensile) strains. One can also consider isolating the strain-induced effects in Eqs. (37) and (38) from the band structure, contained in $v_{\vec{k}}^{\alpha}$, and from the spectral function ρ_G , which accounts for the influence of the Gutzwiller correlations on resistivity. (Changes in the resistivity due to variation of the explicit lattice constants are small.) When we exert a compressive strain, this produces additive changes to the longitudinal resistivity due to in equal parts (1) changes in vertex and (2) T -dependent changes in spectral function, both arising from the enhancement of t_x . Whereas for the transverse resistivity the hopping parameter t_y is unchanged and hence changes to resistivity from the band structure become less important and as a result the transverse resistivity is dominated by strain-induced effects on the spectral function. For this reason, the transverse response to compressive strain is generally smaller in magnitude than the longitudinal response and likewise for a tensile strain both shown in panel (c). We

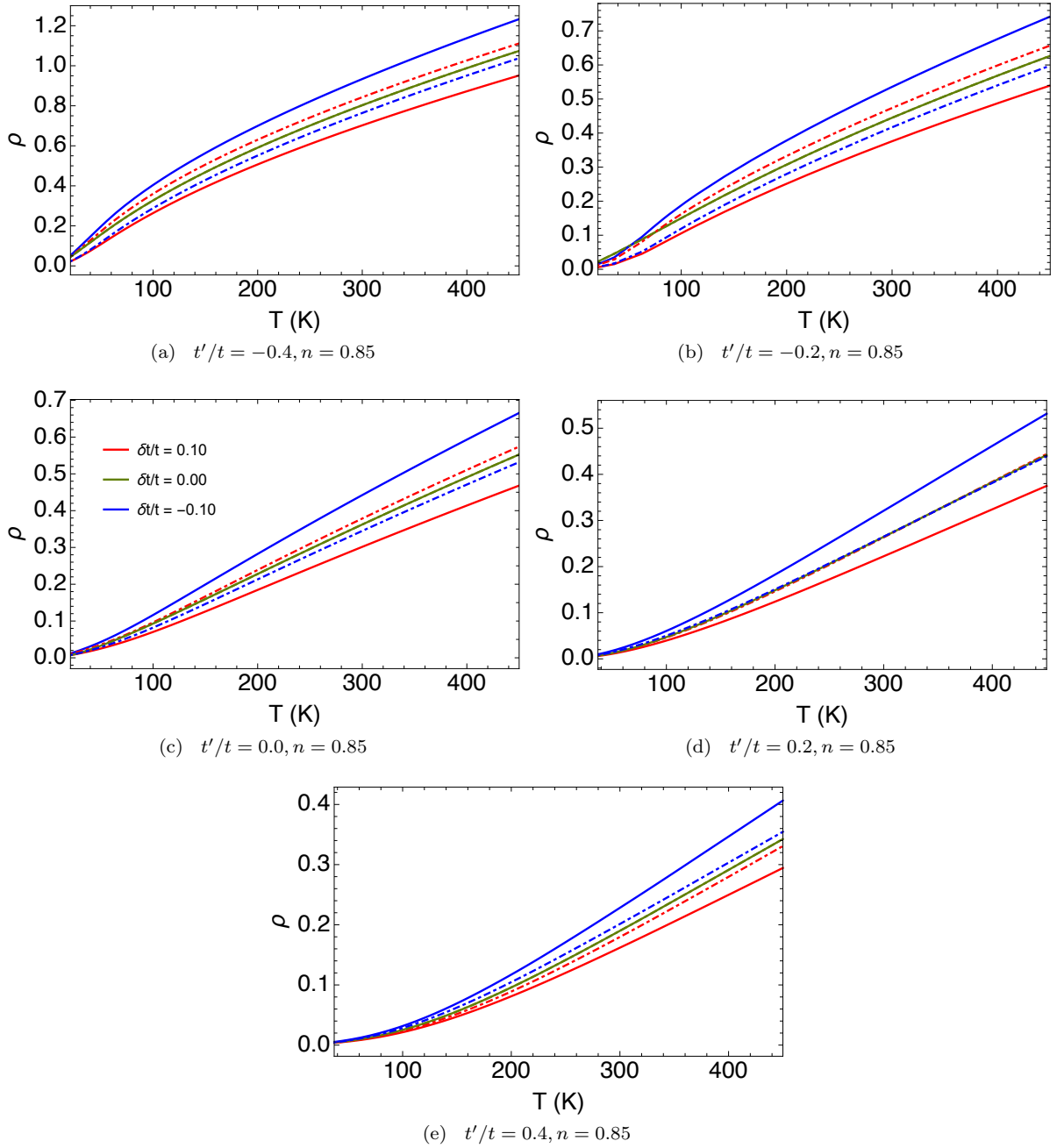


FIG. 1: The longitudinal and transverse resistivities, ρ_{xx} (solid) and ρ_{yy} (dashed) respectively, versus temperature at filling $n = 0.85$, for various t' , and at representative strains. While the green curves are for the unstrained case, the red curves correspond to a compressive strain $\delta t/t = 0.10$ (i.e. $\epsilon_{xx} \sim -.02$), and the blue curves correspond to a tensile strain $\delta t/t = -0.10$ (i.e. $\epsilon_{xx} \sim .02$), if we take $\alpha \sim 5$. All figures share the legend. The resistivity in physical units can be found by $\rho_{\text{physical}} = \rho \times \rho_0$, where $\rho_0 = \epsilon_0 \hbar / e^2 \sim 1.17 \text{ m}\Omega \text{ cm}$.

also find that the transverse strain response has a different sign than the longitudinal one when there is no second neighbor hopping.

Now let us turn on t' . According to Eq. (27), the strain has a longitudinal-like effect, only smaller, on the magnitude of the second neighbor hopping. Turning on a positive t' strengthens longitudinal response and “counters”

the transverse response from t_y hopping. Therefore we see that the longitudinal curves depart further from the unstrained one in panel (d) and (e), and it also explains why the transverse change almost vanish for $t' = 0.2$ in panel (d) and switch to the same sign as the longitudinal one for $t' = 0.4$ in panel (e). Likewise turning on a negative t' weakens the longitudinal response and

enhances the transverse response, so that the longitudinal response gets smaller in panel (a) and (b) while the transverse shifts more explicitly to the same side as $t' = 0$. Further analysis of these effects can be found in the Supplementary Material (SM) [55].

Next we discuss the how strain affects the effective interaction and the characteristic temperature scale. We mainly use the longitudinal resistivity in this discussion because the longitudinal response is more explicit. In our recent work [7,8], a significant finding was the t' dependence of the curvature of the $\rho - T$ lines. We observe that this t' -dependent curvature persists under strain, i.e., the curvature changes from positive (concave up like $+T^2$) to negative (convex up like $-T^2$) as t'/t is varied upward.

Recall that strain is effectively a small change in the hopping parameter, so we ought to expect strain to change the t' dependence of the curvature only quantitatively but not qualitatively. Phenomenologically, varying t' signals a change in the effective Fermi temperature scale T_{FL} where for $T < T_{FL}$ the system is in the Fermi liquid regime $\rho \propto T^2$ and hence has a positive curvature. Moreover, as we decrease t' from positive to negative, the Fermi liquid temperature regime is compressed into a smaller temperature regime down to temperatures where resistivity is usually hidden by the superconducting state. We want to focus on the crossover between Fermi liquid and strange metal which is covered by the following empirical relation

$$\rho \sim C \frac{T^2}{T_{FL} + T}. \quad (39)$$

Here C is a constant that defines the slope of linear regime and T_{FL} marks the crossover from the Fermi-liquid regime. For example when $t' = -0.2t$ as found in typical hole-doped cuprates [56], we observe that a compressive strain extends the Fermi-liquid regime for the longitudinal resistivity, and flipping the strain reduces the Fermi-liquid regime. Qualitatively speaking, a compressive strain enhances the longitudinal hopping so that the effective interaction reduces relatively to the hopping. Likewise, a tensile strain increases the effective interaction in the unit of longitudinal hopping and suppress the Fermi liquid temperature scale. Besides, we observe that a compressive strain suppresses the linear constant C while a tensile strain enhances it, as shown more obviously in Fig. 2. That can be verified in the experiment by measuring the slope of $\rho - T$ for a *strange metal* under strain.

2. Susceptibilities for anisotropic resistivities

It has been argued [1] that cuprates are candidates for an electron nematic phase, in which nematic order might coexist with high temperature superconductivity, that is, the electronic system breaks a discrete rotational symmetry while leaving the translational symmetry intact. Here the normalized resistivity response plays the role of the

order parameter in the phase transition. Since it is possible to experimentally identify continuous phases transitions through observation of a diverging thermodynamic susceptibility across a phase boundary this makes the temperature profile of elastoresistance, i.e. normalized resistivity response with respect to an arbitrary strain, an interest observable to explore. For that reason, we shall examine linear response function for the longitudinal and transverse components of the elastoresistivity tensor constructed in terms of the hopping strain as:

$$\chi_{XX} \equiv -\left(\frac{\rho'_{xx} - \rho_{xx}}{\rho_{xx}}\right) / \left(\frac{\delta t}{t}\right), \quad (40)$$

$$\chi_{YY} \equiv -\left(\frac{\rho'_{yy} - \rho_{yy}}{\rho_{xx}}\right) / \left(\frac{\delta t}{t}\right), \quad (41)$$

respectively. The susceptibility as defined is positive if compression along x-axis leads to a reduction of the resistivity in the specified direction. We note the connection of these susceptibilities with the nematic susceptibility Eq. (1) on using Eq. (28) as

$$\chi_{nem} = \alpha \lim_{\epsilon_{xx} \rightarrow 0} \chi_{XX}. \quad (42)$$

We compute the susceptibility for small values of strain $\delta t/t \gtrsim .05$. However, even these values of strain pick up some non-linear components of the response function. These are also of interest, and we comment on these below.

The linear response function for strain-resistivity curves is plotted as a function of temperature in Fig. 2 for the longitudinal and transverse components at optimal density $n = 0.85$ for various t' and $\delta t/t$. Note that since the resistivity vanishes as $T \rightarrow 0$, there is an enhancement of the normalized susceptibility at low- T .

In Fig. 2, subfigures (a,c,e,g,i) we see that the linear response function for the longitudinal resistivity χ_{XX} is mostly positive and shows non-linear (in $\delta t/t$) behavior at a fixed T (as can be identified by the separation of the strain curves) with respect to strain across the entire temperature range. This non-linearity will be measured directly in Fig. 5 for $t' = -0.2$. The response function for $T \gtrsim 100K$ is highly ordered in that varying the strain from positive (compressive) to negative (tensile) increases the strength of the response function for all t' . Conversely as we cool the system, we observe that strain dependence of the response function becomes increasingly non-linear, i.e., showing a wider separation between strain curves, the forms of which are strongly t' dependent. Now if we vary t' to survey the range of cuprate materials, we find at low- T for hole-like ($t' < 0$) materials a significant enhancement in and an inversion of the strain dependence that is absent in electron-like ($t' > 0$) materials, though for both material types the strength of the response function remains approximately invariant at high- T .

We next discuss the transverse linear response function χ_{YY} shown in Fig. 2, subfigures (b,d,f,h,j). This response is potentially interesting since the affects of strain on the

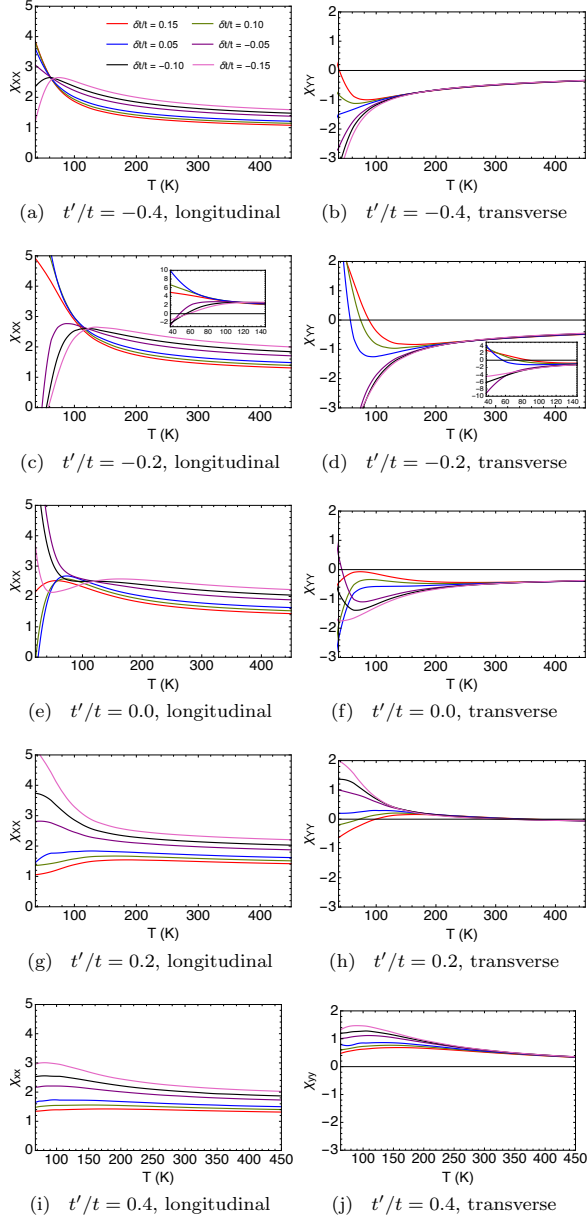


FIG. 2: The longitudinal [Eq. (40)] and transverse [Eq. (41)] strain-resistivity susceptibilities versus temperature at filling $n = 0.85$, for various t'/t and $\delta t/t$. All figures share a legend. For various $\delta t/t$, the susceptibilities χ_{xx} for $T \gtrsim 100$ approach each other in two sets, one for $\delta t/t > 0$ and another slightly displaced set for $\delta t/t < 0$. They splay apart at low T thus displaying strong non-linearity in the Fermi liquid regime. The susceptibilities χ_{yy} approach a single set for $T \gtrsim 100$ and splay apart for low T thus also displaying strong non-linearity in the Fermi liquid regime.

band structure are found to play a less significant role, hence the correlation effects dominate. We find that the features of transverse response function are different from that of the longitudinal response function mainly in two ways: (1) the χ_{yy} collapses at high- T , showing strong linearity with respect to the strain and (2) it changes sign

from negative to positive as we vary t'/t across 0.2 from below, consistent with Fig. 1. Measurements confirming this linear behavior and sign change would be potentially interesting results.

3. Resistivity with non-zero J

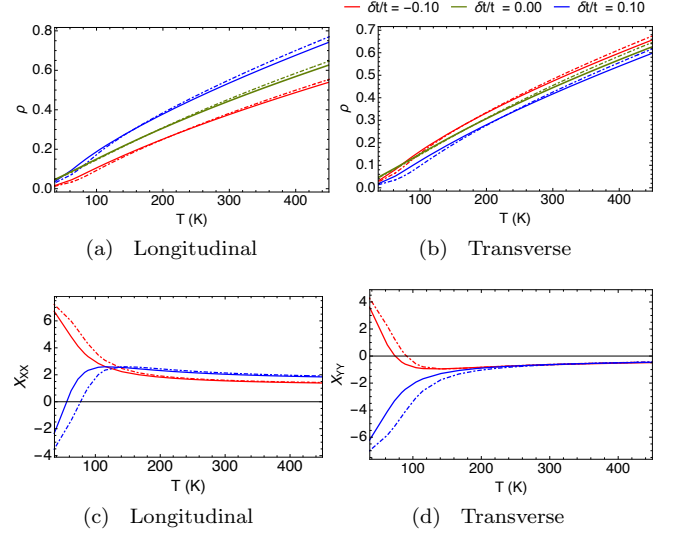


FIG. 3: (a)-(b) The strain-induced resistivity at optimal filling $n = 0.85$, $t'/t = -0.2$ for three representative strain types with exchange parameter $J = 0.0$ (solid) and $J = 0.17$ (dashed). (c)-(d) The strain-resistivity susceptibility for the same parameter set as above. All figures share a legend. We note that a non-vanishing J enhances somewhat the magnitude of the susceptibilities in the low temperature Fermi liquid regime.

In this section we examine the role of exchange parameter J (nearest neighbor exchange energy) on resistivity and the susceptibilities, setting $J = 0.17t$ which is the typical value for LSCO cuprate materials [48]. We take $J = t^2/U$ where U is the on site energy of the Hubbard model and U does not vary with strain and hence $\delta J = 2(\delta t/t)J$ [47]. Now, if we turn on the exchange parameter J , we find that at low temperatures the resistivity is reduced by the exchange energy and at high temperatures the resistivity is slightly enhanced as seen in Fig. 3 panels (a) and (b). In panels (c) and (d) we see the longitudinal and transverse susceptibility with exchange interaction is further enhanced at low-temperatures whereas at higher temperatures the response is unchanged. The J effects are magnified in the low- T response since $\rho \rightarrow 0$ as $T \rightarrow 0$. We can say the effects of J on the response are negligible at high- T .

4. Susceptibilities for A_{1g} and B_{1g} irreps

Experimentally, it is possible to identify the irrep to which the order parameter belongs by applying a strain with a particular irrep of strain and searching for a divergence in the temperature profile. In the case of uniaxial strain along the x-axis the strain can be decomposed into the A_{1g} and B_{1g} irreps. In this section we examine the strain-resistivity linear response function for the A_{1g} and B_{1g} irreps defined in terms of the hopping strain as

$$\begin{aligned}\chi_{A_{1g}} &\equiv -\left(\frac{\rho'_{xx} + \rho'_{yy} - 2\rho'_{xx}}{2\rho_{xx}}\right) / \left(\frac{\delta t}{t}\right) = \frac{\chi_{XX} + \chi_{YY}}{2}, \\ \chi_{B_{1g}} &\equiv -\left(\frac{\rho'_{xx} - \rho'_{yy}}{\rho_{xx}}\right) / \left(\frac{\delta t}{t}\right) = \chi_{XX} - \chi_{YY},\end{aligned}\quad (43)$$

respectively.

In Fig. 4 we present the normalized strain-resistivity response functions at optimal density $n = 0.85$ for various t' and $\delta t/t$. In this picture the A_{1g} and B_{1g} irreps play the roles of a center of mass coordinate and a relative coordinate, respectively. Together the two susceptibilities characterize the shift of in-plane resistivity as a result of an arbitrary in-plane strain. Recall that since the resistivity vanishes as $T \rightarrow 0$, the A_{1g} and B_{1g} susceptibilities are also enhanced at low- T .

Examining the A_{1g} susceptibilities in Fig. 4 (a,c,e,g), one important feature stands out, namely, that for $T \gtrsim 100\text{K}$ the response function is positive for all t' and strains $\delta t/t$. This indicates that increasing a tensile (compressive) strain for $T \gtrsim 100\text{K}$ enhances (suppresses) the average of the anisotropic resistivities.

We also see that at $T \sim 100\text{K}$ with hole doping, i.e. $t' \leq 0$, the normalized susceptibilities become independent of the strain, and hence the response is in the linear regime (signaled by the convergence of all strain curves). The non-linear response at lower T is interesting and potentially observable in experiments with varying strain. On the other hand for electron doping, i.e. $t' > 0$, we see non-linear behavior even at high T . Its origin is the extended Fermi-liquid regime which has a higher crossover temperature scale. Summarizing, we find that the early departure from Fermi liquid behavior into a strange metallic behavior in the hole doping favors an apparent linear response above 100K due to a change in scale. Conversely we expect to see non-linearity extending to much higher T 's in electron-doped systems.

From Fig. 4, we observe that the B_{1g} susceptibilities for $T < 100\text{K}$ are strongly dependent on the value of t' of the system. We find in hole-like materials ($t' \lesssim 0.0$) there is a strong enhancement (the details of which depend on the $\delta t/t$) in the susceptibility at low- T . In contrast, this feature is absent in electron-like materials ($t' > 0.0$) where there is weaker correlation, higher T_{FL} , and hence stronger quasiparticles.

Focusing on the strain dependence, we see that at high- T the susceptibilities are relatively insensitive to t' and generally increases as we vary from a compressive

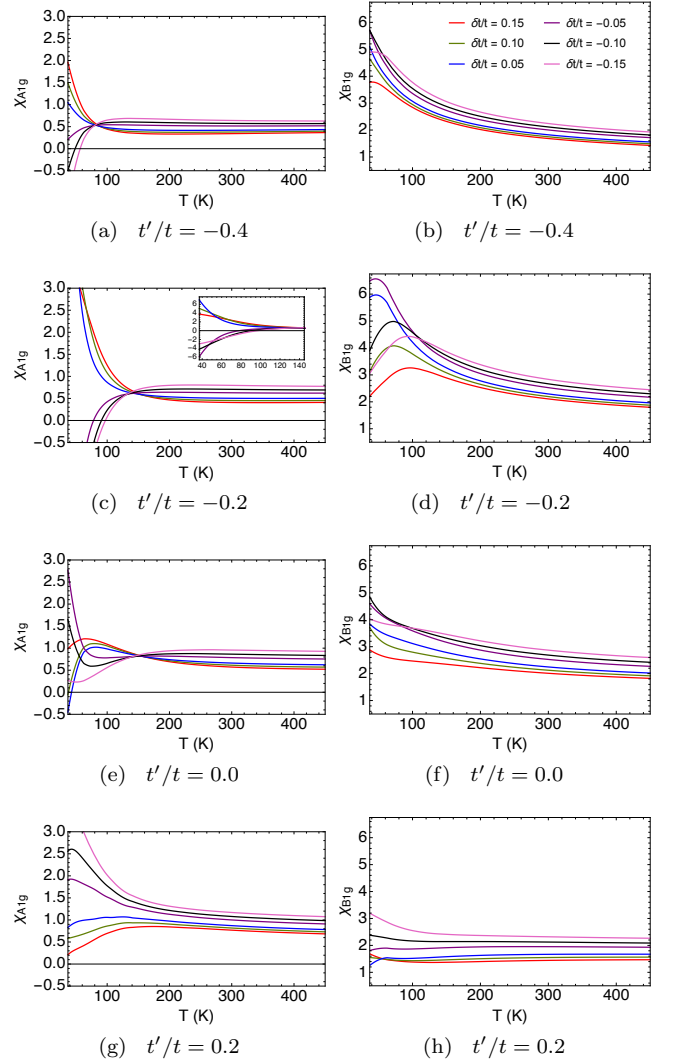


FIG. 4: The normalized strain-resistivity susceptibilities from Eq. (43) versus T for the A_{1g} and B_{1g} irreducible representations at filling $n = 0.85$ at various t' and $\delta t/t$. All the figures share a legend. For various $\delta t/t$, and for $T \gtrsim 100$ all the susceptibilities approach each other in two sets, one for $\delta t/t > 0$ and another slightly displaced set for $\delta t/t < 0$. They splay apart at low T thus displaying strong non-linearity in the Fermi liquid regime.

to a tensile strain. There is also asymmetry in rate of change of susceptibilities between a compressive and tensile strain as $|\delta t/t|$ is varied, i.e., the response function changes more rapidly for tensile than compressive strains. Therefore the degree of anisotropy is higher for tensile strain than compressive strains of equal magnitude.

Also, the B_{1g} curves under compressive strain ($\delta t/t > 0$) are closer to each other than those under tensile strain for electron-doped systems, yet this spacing difference is less obvious in the hole-doped case. It means that a tensile response tends to show stronger non-linearity, especially in electron-doped systems.

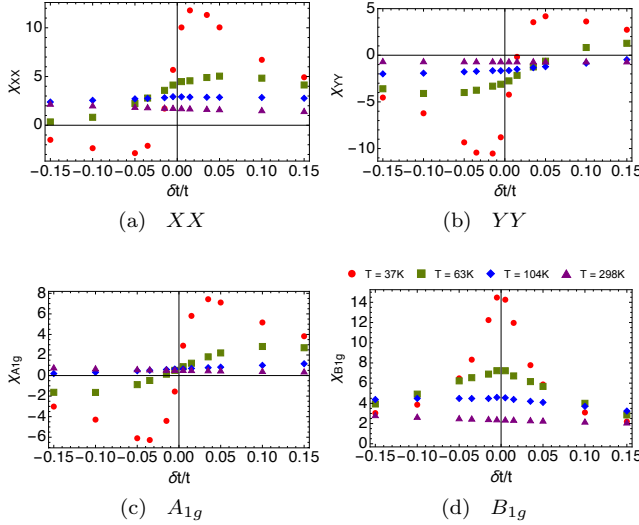


FIG. 5: The strain-resistivity susceptibilities for various symmetries as a function of strain $\delta t/t$ at filling $n = 0.85$ and $t'/t = -0.2$. (a) XX, longitudinal, Eq. (40); (b) YY, transverse, Eq. (41); (c) A_{1g} irrep, Eq. (43); (d) B_{1g} irrep, Eq. (43). The susceptibilities are relatively strain independent above 100K, but show strong non-linearity at low T. It is noteworthy that for the lowest T shown, the susceptibilities χ_{xx} , χ_{yy} , $\chi_{A_{1g}}$ change sign at or close to $\delta t/t = 0$. At higher T this change of sign is lost. The behavior of the nematic susceptibility $\chi_{nem} = \lim_{\epsilon_{xx} \rightarrow 0} (\alpha \chi_{xx})$ at low T has thus the potential for a change of sign, depending on how we choose a sufficiently small $|\epsilon_{xx}|$ or $|\delta t/t|$ for the purpose of taking the limit $\lim_{\epsilon_{xx} \rightarrow 0}$.

5. Susceptibilities versus strain

In Fig. 5, we display the strain-resistivity response functions versus hopping strain for various symmetries at $t' = -0.2t$ and $n = 0.85$ (which is roughly the parameter set for LSCO cuprate material [56] at optimal density) at four representative temperatures.

Here we approximate the variance in the linear response function as follows

$$\chi(T) = c_0(T) + c_1(T)(\delta t/t) + c_2(T)(\delta t/t)^2 + \dots \quad (44)$$

In panel (a) and (b) we have longitudinal and transverse linear response functions, respectively, showing non-linear behavior at low temperature which becomes more linear (as indicated by horizontal line) as the system warms. This non-linear behavior at low-T can be understood as a result of the increasing importance of correlations as the system is cooled. Although the longitudinal and transverse response functions differs considerably in magnitude, the curves are approximately symmetric under inversion of the axes. In panels (a), (b) and (c) there is a wave-like oscillation which indicates the presence of higher order terms, e.g., the $T = 37K$ curve in panel (a) appears to have $(\delta t/t)^3$ term competing with a linear term. Another interesting result we find that as the

system cools the B_{1g} response function appears diverge at $\delta t/t = 0$ as $T \rightarrow 0$ suggests that any deviation from the point group symmetry of the square lattice produces a finite resistivity response.

B. Kinetic Energy for an x-axis strain

In this section we explore the kinetic energy anisotropy induced by strain along the x-axis using ECFL theory. Since the anisotropic kinetic energy can be related to measurements of the optical conductivity using the f-sum rule on the t - t' - J model, this makes it an another interesting observable to explore.

The total kinetic energy for a system under strain is computed as

$$K_{\text{tot}} = \left\langle \int_{-\infty}^{\infty} \rho_G(\vec{k}, \omega) \epsilon_{\vec{k}} d\omega \right\rangle_k. \quad (45)$$

This may be decomposed as follows:

$$K_{\text{tot}} = K_{xx} + K_{yy} + K_{xy}, \quad (46)$$

where the cross kinetic energy K_{xy} comes from the second neighbor interactions and is related to the dynamic Hall conductivity. Additional information on the total kinetic energy can be found in the SM [55]. The longitudinal, transverse and cross kinetic energies are given by

$$K_{xx} = \left\langle \int_{-\infty}^{\infty} d\omega \rho_G(\vec{k}, \omega) \epsilon_{k_x} \right\rangle_k \quad (47)$$

$$K_{yy} = \left\langle \int_{-\infty}^{\infty} d\omega \rho_G(\vec{k}, \omega) \epsilon_{k_y} \right\rangle_k \quad (48)$$

$$K_{xy} = \left\langle \int_{-\infty}^{\infty} d\omega \rho_G(\vec{k}, \omega) \epsilon_{k_{xy}} \right\rangle_k \quad (49)$$

where

$$\epsilon_{k_x} = -2t_x \cos(k_x a) \quad (50)$$

$$\epsilon_{k_y} = -2t_y \cos(k_y b) \quad (51)$$

$$\epsilon_{k_{xy}} = -4t_d \cos(k_x a) \cos(k_y b). \quad (52)$$

In the t - t' - J model the anisotropic kinetic energies K_{α} , where $\alpha = xx, yy$ and xy , are related to the optical conductivity σ_{α} by the following sum rule

$$\Re \int_0^{\infty} \sigma_{\alpha}(\omega) d\omega = -K_{\alpha} e^2, \quad (53)$$

where e is the electrical charge. $K_{\alpha} e^2$ sets the scale of the optical conductivity, i.e.,

$$-\frac{1}{K_{\alpha} e^2} \Re \int_0^{\infty} \sigma_{\alpha}(\omega) d\omega = 1. \quad (54)$$

The optical conductivity in the DC limit $\sigma_{\alpha}(0)$ relates to the DC resistivity as follows: $\rho_{\alpha}(0) = 1/\sigma_{\alpha}(0)$. For the anisotropic kinetic energy, we calculate and quote the following objects:

- K'_{xx} is the strained version of longitudinal kinetic energy.
- K'_{yy} is the strained version of transverse kinetic energy.
- We call K_{xx} without a prime the tetragonal result. It is the same as K_{yy} .
- We present A_{1g} :

$$-\frac{K'_{xx} + K'_{yy} - 2K_{xx}}{2K_{xx}(\delta t/t)} \text{ vs } T$$

- We present B_{1g} : $-(K'_{xx} - K'_{yy})/(K_{xx}\delta t/t)$ vs T

1. Raw kinetic energies

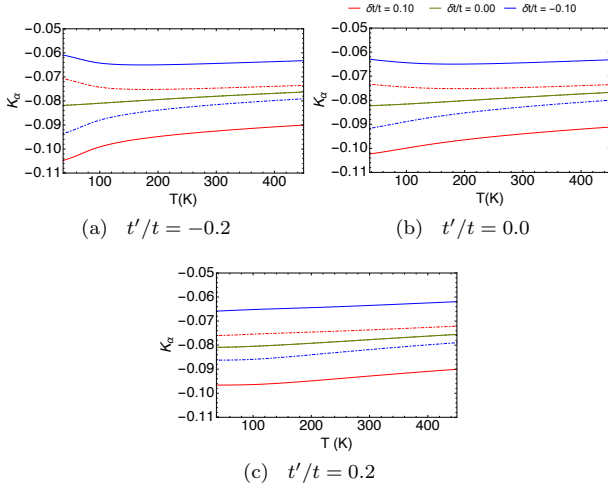


FIG. 6: Anisotropic kinetic energies K_α versus T for K_{xx} (solid) and K_{yy} (dashed) at filling $n = 0.85$, for various t' and at three representative strains: compressive strain, no strain, and tensile strain. Note that $K_{xx} = K_{yy}$ in absence of strain. All figures share a legend.

From Eq. (47) we calculate the anisotropic kinetic energies K_α as a function of temperature at optimal density for a representative range of cuprate materials t' and hopping strains $\delta t/t$ as shown in Fig. 6. The main observation is that a compressive (tensile) strain suppresses (enhances) the longitudinal kinetic energy and vice versa for the transverse kinetic energy response with a smaller magnitude of variation. The variation in the longitudinal kinetic energy can be understood as combination of changes in the band structure parameter t_x and correlations. On the other hand, the transverse kinetic energy is dominated by changes to the correlation function since the parameter t_y is unmodified by x-axis strain. There is little T -dependence with exception to a slight broadening of the range of the response at low- T as the T_{FL} is reduced. The t' -dependence is also weak because K_{xx}

and K_{yy} does not explicitly depend on t' but through the spectral function.

2. Strain-kinetic-energy susceptibilities

In analogy with elastoresistance, we compute the so-called normalized strain-kinetic-energy response function, which measures the change in kinetic energy with respect to a strain. We shall focus on the normalized strain-kinetic-energy response functions for the A_{1g} and B_{1g} irrep since measurements of these symmetries are sensitive to a break in the 4-fold rotation symmetry of a square lattice. Explicitly the response functions are defined in terms of hopping strain as

$$M_{A_{1g}} \equiv -\left(\frac{K'_{xx} + K'_{yy} - 2K_{xx}}{2K_{xx}}\right) / \left(\frac{\delta t}{t}\right), \quad (55)$$

$$M_{B_{1g}} \equiv -\left(\frac{K'_{xx} - K'_{yy}}{K_{xx}}\right) / \left(\frac{\delta t}{t}\right), \quad (56)$$

where the sign is imposed so that susceptibility defined in terms of hopping strain matches its counterpart defined in terms of conventional strain. Fig. 7 displays the normalized strain-kinetic-energy susceptibilities as a function of temperature for the A_{1g} and B_{1g} irrep at optimal density for various t' and $\delta t/t$. The A_{1g} irrep susceptibility signals a change in the sum of anisotropic kinetic energies $K_{xx} + K_{yy}$ with respect to the hopping change. The A_{1g} susceptibility shows that tuning the strain from tensile to compressive increases rather uniformly the magnitude of the anisotropic kinetic energy, i.e., strain enhances the overall optical weight from Eq. (53). Analysis of the longitudinal and transverse components are in the SM [55].

The B_{1g} susceptibility is characterized as the difference in the kinetic energies $K_{xx} - K_{yy}$ with respect to the hopping change. Thus a non-zero value for the B_{1g} irrep signals an anisotropy between the two directions. We observe that the response function for the B_{1g} irrep is strongly t' dependent. For $t' = -0.4$, the response functions is nearly linear at all temperatures. We point out a curious feature for $t' = -0.2$ curve where at high- T the system is linear whereas at low- T the system is non-linear, but it nearly symmetric with respect to a compressive or tensile strain of similar magnitude. At high- T for all t' the system is monotonic with respect to strain. For $t' \geq 0$ there is little variation in the response function across the temperature range and it appears to become increasingly non-linear as the system is warmed due to the reduction in the scale of variation.

3. Strain-kinetic-energy susceptibility versus strain

We now present strain-kinetic-energy susceptibility as a function of strain at optimal density ($n = 0.85$) and

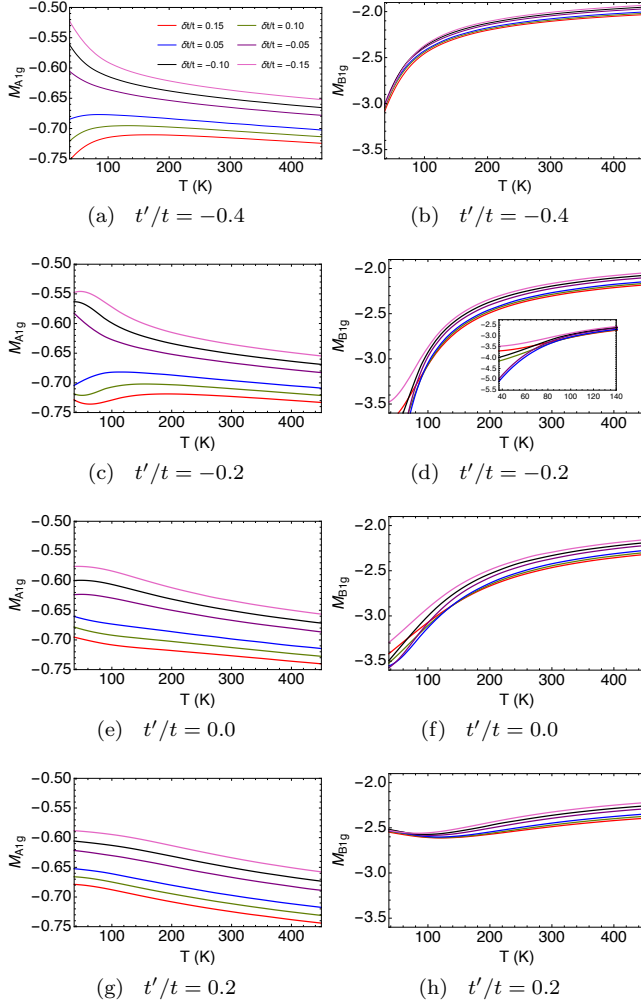


FIG. 7: The normalized strain-kinetic-energy susceptibilities vs T for the A_{1g} and B_{1g} irrep as defined in Eqs. (55) and (56) at filling $n = 0.85$, for various t' and $\delta t/t$. All figures share a legend.

$t' = -0.2t$ for XX , YY , A_{1g} , B_{1g} symmetries at various T (see Fig. 8), where we define the longitudinal and transverse response functions as

$$M_{XX} \equiv -\left(\frac{K'_{xx} - K_{xx}}{K_{xx}}\right) / \left(\frac{\delta t}{t}\right), \quad (57)$$

$$M_{YY} \equiv -\left(\frac{K'_{yy} - K_{yy}}{K_{xx}}\right) / \left(\frac{\delta t}{t}\right). \quad (58)$$

respectively. Like the resistivity case, $M_{A_{1g}} = 0.5 \times (M_{XX} + M_{YY})$ and $M_{B_{1g}} = M_{XX} - M_{YY}$.

We find that at low temperatures, decreasing the magnitude of the strain increases the strength of the longitudinal response function in panel (a) and the response function is symmetric with respect to both strain types. The transverse response function in panel (b) shows a similar symmetry between tensile and compressive strains with a flipped sign. Therefore we find that a compressive strain for the A_{1g} response function [panel

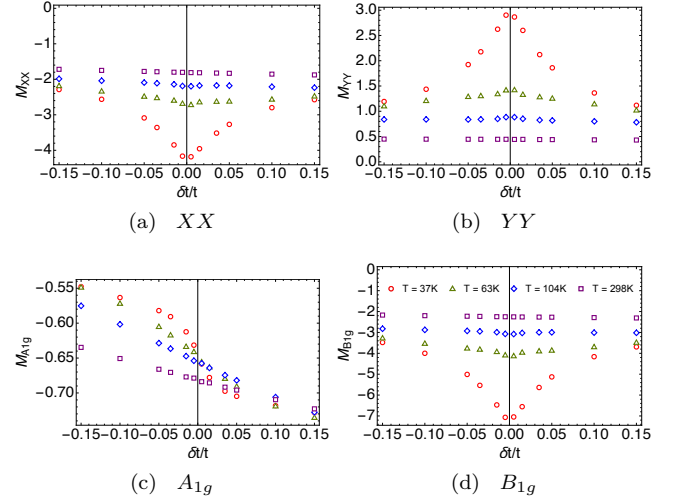


FIG. 8: The strain-kinetic-energy susceptibilities versus $\delta t/t$ at filling $n = 0.85$ and $t'/t = -0.2$ at four representative temperatures. All figures share a legend. (a) XX , longitudinal, Eq. (57); (b) YY , transverse, Eq. (58); (c) A_{1g} irrep, Eq. (55); (d) B_{1g} irrep, Eq. (56).

(c)] depletes the in-plane optical weight and vice versa for a tensile strain. The B_{1g} response function is similar to the longitudinal and transverse only more intensive and it signals an enhanced (suppressed) anisotropy between in-plane kinetic energies for a compressive (tensile) strains. In all cases the response function is approximately linear at room temperature (297K) and becomes increasingly non-linear as the system cools. In comparing panels (b), (c), and (d) we see strong similarity between their respective responses. This is expected since strain merely shifts kinetic energy versus temperatures curves up and down. Also, it appears to diverge for small strains as $T \rightarrow 0$.

C. The local density of states for an x-axis strain

The local density of states (LDOS) is also very interesting since it can be measured using STM probes. We present results on how the LDOS changes with strain, and the related susceptibilities. We argue that if experiments are done on resistivity variation as well as LDOS variation with strain, we can bypass the need for measuring strain accurately and of estimating the parameter α in Eq. (19). The LDOS is calculated as $\rho_{\text{Gloc}}(\omega) = \langle \rho_G(\vec{k}, \omega) \rangle_k$ where averaging over the Brillouin zone is implied, and $G \rightarrow g$ is the free Green's function (i.e., band structure) which gives the bare LDOS and the ECFL Green's function $G \rightarrow \mathcal{G}$ gives the LDOS for the t - t' - J model.

In this section we calculate the normalized change in the local density of states and quote the following:

$$\bullet \rho'_{g\text{loc}}(\omega) = \langle \rho_g(\vec{k}, \omega) \rangle_k \text{ is the bare LDOS for a strain}$$

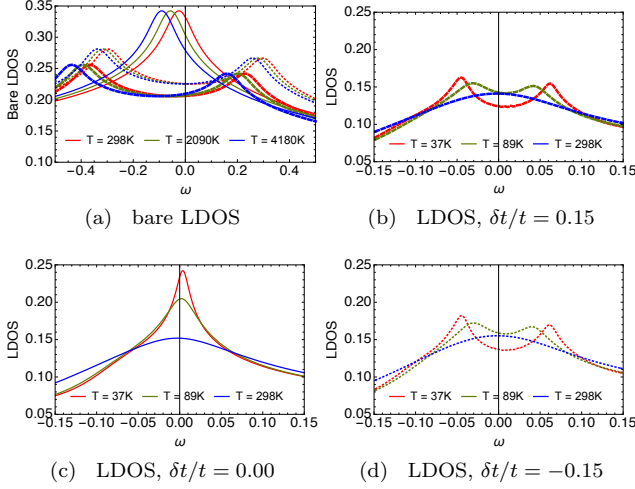


FIG. 9: The local density of states for (a) the non-interacting (band-structure) and (b)-(d) interacting system (t - J model) at optimal filling ($n = 0.85$), $t' = -0.2t$, for various temperatures and at three characteristic strains: $\delta t/t = 0.15, 0.00, -0.15$ (thick dashed, solid, thin dashed).

along the x-axis

- $\rho'_{g\text{loc}}(\omega) = \langle \rho_g(\vec{k}, \omega) \rangle_k$ is the interacting LDOS for an x-axis strain
- $\rho_{g\text{loc}}$ without a prime refers to the tetragonal result and similarly for $\rho_{g\text{loc}}$.
- We present $(\rho'_{g\text{loc}} - \rho_{g\text{loc}})/(\rho_{g\text{loc}}\delta t/t)$ vs ω
- We present $(\rho'_{g\text{loc}} - \rho_{g\text{loc}})/(\rho_{g\text{loc}}\delta t/t)$ vs ω

1. T variation

In Fig. 9, we display the LDOS at optimal density ($n = 0.85$) and $t' = -0.2$ for various temperatures at three characteristic strains: a compressive strain (thick dashed), unstrained (solid) and tensile strain (thin dashed). We compare the LDOS for a non-interacting system [panel (a)] to a system with electron-electron interaction [panels (b)-(d)]. We find over large temperature scales that curves for the bare LDOS shifts to left along the ω -spectrum upon warming, leaving the line shape intact. In contrast with the bare LDOS, we see that warming the LDOS for the interacting system in panel (c) completely smooths and broadens the LDOS peaks for all strains, and slightly shifting them left. This is consistent with previous findings that interactions significantly lower the Fermi liquid temperature T_{FL} [7]. We note that strain inverts the LDOS peak at low- T , leaving behind a pair of cusps at a reduced height. This is an artifact of the anisotropy of hopping parameters since it also shows up in the bare case.

2. J variation

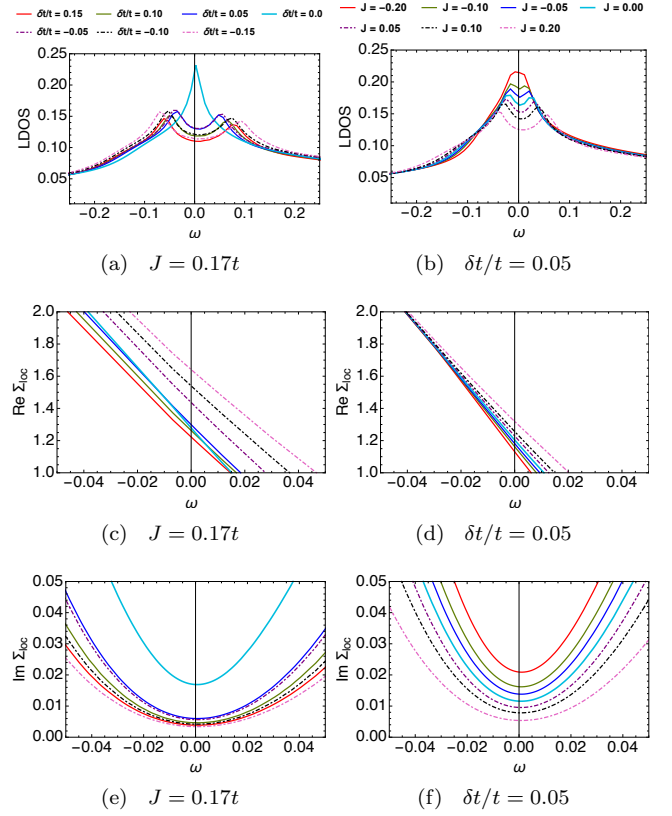


FIG. 10: (a,b) The LDOS; (b,c) real part of local Dyson self-energy; (e,f) the imaginary part of local Dyson self-energy for parameter set $n = 0.85$, $T = 37\text{K}$, $t' = -0.2t$ with varying $\delta t/t$ (LHS) and varying J (RHS). Figures (a,c,e) and (b,d,f) share a legend, respectively.

In Fig. 10, we turn on the exchange parameter J and examine the LDOS. We also find it useful to examine the self-energy of the system. We define the Dyson self-energy Σ as

$$\mathcal{G}(k) = \frac{1}{\omega + \mu - \epsilon_{\vec{k}} - \Sigma(k)} \quad (59)$$

Here we use the shorthand $\Sigma = \Sigma' + i\Sigma''$ to denote the real and imaginary parts of a complex function. In terms of the spectral function, self-energy imaginary part is

$$\Sigma''(k) = \frac{-\pi\rho_{\mathcal{G}}(k)}{[\mathcal{G}'(k)]^2 + [\pi\rho_{\mathcal{G}}(k)]^2}, \quad (60)$$

where $\Re\mathcal{G} = \mathcal{G}'$ is found by taking the Hilbert transform of $\Im m\mathcal{G} = \mathcal{G}''$ and we can find Σ' in the same manner. In Figure 10 (c-f) we display the Dyson self-energy averaged over the Brillouin zone $\Sigma_{\text{loc}}(\omega) = \langle \Sigma(\vec{k}, \omega) \rangle_k$.

Turning on the exchange parameter in Fig. 10 (a) has a small, but visible effect on LDOS at low- ω when compared to S-Fig. 6(b) of the SM [55]. For panel (c)

we see that varying strain from compressive ($\delta t/t > 0$) to tensile ($\delta t/t < 0$) shifts the average quasi-particle states to higher energies and panel (e) shows that increasing the intensity of the strain produces quasi-particles with higher and sharper peaks. In panels (b,d,f) we see that varying J from ferromagnetic (negative) to anti-ferromagnetic (positive) splits a single LDOS peak into two, shifts the average quasi-particle states to higher energies, and narrows the quasi-particle peaks.

3. t' variation

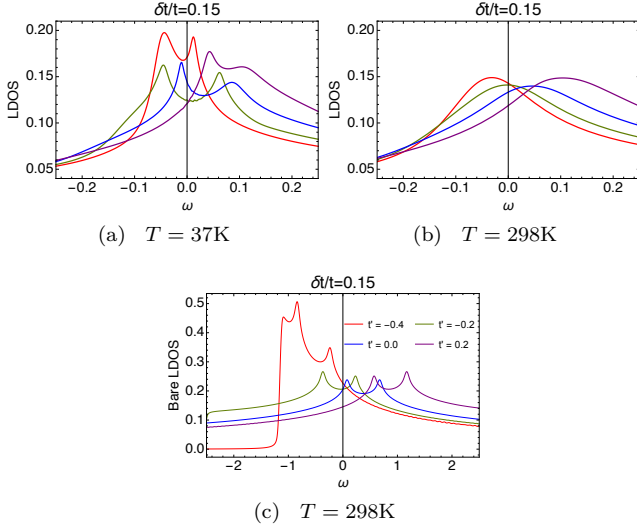


FIG. 11: The local density of states versus frequency at optimal filling ($n = 0.85$), for a compressive strain ($\delta t/t = 0.15$) at various t' . (a)-(b) The interacting system (t - t' - J model) at $T = 37\text{K}$ and $T = 298\text{K}$, respectively. (c) The non-interacting (band-structure) system at $T = 298\text{K}$. All figures share the same legend.

In Fig. 11, we examine the LDOS from a different vantage point by looking at the t' dependence for a system at optimal density ($n = 0.85$), for a compressive strain of $\delta t/t = 0.15$, at various t'/t . In panel (c), we show the bare LDOS at room temperature as a reference for the interacting system. In panels (a) and (b), we display interacting system at $T = 37\text{K}$ and $T = 298\text{K}$, respectively. Upon inspection it appears the primary role that t' plays is to shift the energy band along the spectrum. As previously noted, warming the interacting system to room temperature smooths and broadens the characteristic LDOS peaks for all strain types and at all t' while leaving their position in the spectrum fixed. Even though the relative position of different t' curves remain unchanged as the interactions are turned on, we note that strong correlations renormalizes the bare band into a smaller energy region. Comparing panels (a) and (b) fixed at $t' = -0.4, -0.2$, we observe that LDOS peak height is more strongly suppressed at a lower t' . This

is consistent with previous studies [8] on the unstrained interacting system, and it indicates that a smaller t' has a lower Fermi-liquid temperature scale and hence it is less robust to heating. For further analysis of the strain dependence see the SM [55].

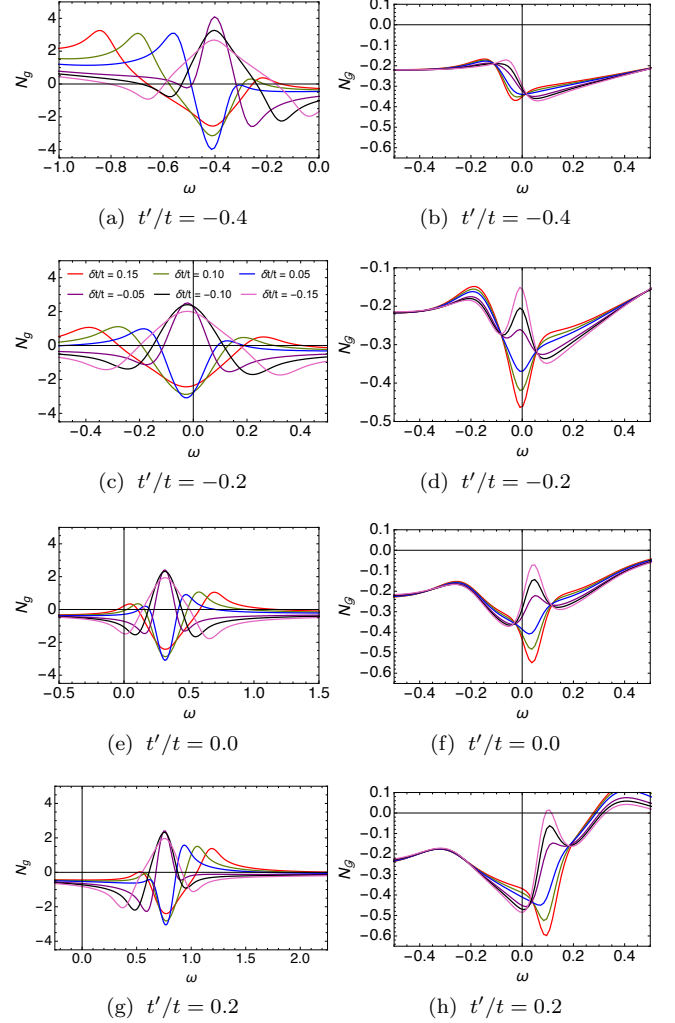


FIG. 12: The LDOS susceptibility versus frequency at optimal filling $n = 0.85$, at room temperature ($T = 297\text{K}$), for various t' and $\delta t/t$. The non-interacting (band-structure) system (LHS) and interacting system (t - t' - J model) (RHS) from Eq. (61) and Eq. (62), respectively. All the figures share a legend.

4. Susceptibilities

Next, we examine the normalized response function of LDOS of the non-interacting and interacting system,

respectively, defined as

$$N_g \equiv \left(\frac{\rho'_{gloc} - \rho_{gloc}}{\rho_{gloc}} \right) / \left(\frac{\delta t}{t} \right), \quad (61)$$

$$N_G \equiv \left(\frac{\rho'_{Gloc} - \rho_{Gloc}}{\rho_{Gloc}} \right) / \left(\frac{\delta t}{t} \right). \quad (62)$$

In Fig. 12, we plot the LDOS susceptibility for a non-interacting and interacting system at room temperature at optimal density for various t' . We observe that the response function is linear at all frequencies except near the LDOS peak and, although not shown in the figure, at the band edges. Regardless of the presence of interaction, we note that the susceptibility is enhanced by tensile strain near the LDOS peak and reduced by a compressive strain.

5. Susceptibility versus strain

Changing up the perspective, we explore the LDOS susceptibility now as a function of strain, at four representative frequencies as seen in Fig. 13. We can approximate the variance in the linear response function in Eqs. (61) and (62) as

$$N(T) = c_0(T) + c_1(T)(\delta t/t) + c_2(T)(\delta t/t)^2 + \dots \quad (63)$$

where c_0 is the linear term, c_1 is the second order term, and c_2 is the third order term of the response. We see that for the bare LDOS, Fig. 13(a), at $\omega = 0.45$ the system is nearly linear with $c_0 \approx -0.5$ and $c_1 \approx 3$. The other presented frequencies appear to be non-linear with significant second and third order terms. The LDOS susceptibility for interacting system [panel (b)] appears to be nearly linear everywhere except at the location of LDOS peak ($\omega = 0$) which has a strong quadratic response, suggesting that at temperatures relevant to experiments non-linear behavior is only observable at energies near the Fermi surface. Note that the second order scheme used here is good for low energies but somewhat less reliable at high energies, $|\omega| \gtrsim k_B T_{FL}$.

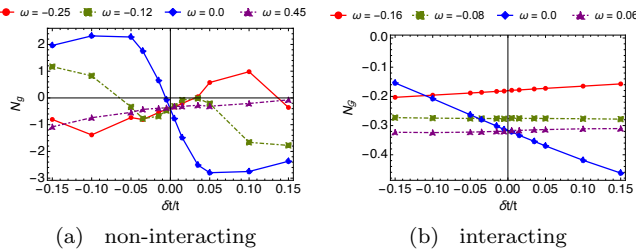


FIG. 13: The LDOS susceptibility versus strain at optimal filling $n = 0.85$, at room temperature ($T = 298K$), for $t' = -0.2t$, at a few representative frequencies ω in units of t . (a) The non-interacting system (band-structure) in Eq. (61). (b) The interacting system (t - t' - J model) in Eq. (62).

IV. SUMMARY AND COMMENTS

A. Summary

In this work, we have applied the ECFL theory to study the effect of small strain on the resistivity, kinetic energy, LDOS and their associated susceptibilities in the t - t' - J model Eq. (2) with various t' at $n = 0.85$. These results are expected to be relevant to cuprate superconductors, especially single layered materials, where the calculated unstrained resistivities are in good accord with the experimental data [6].

Based on comparisons carried out earlier, the second order scheme of ECFL used here is expected to be reasonable in the density range $0.85 \gtrsim n \gtrsim 0.80$ spanning an experimentally accessible range in cuprates. With improvements in the theoretical scheme, we expect that while resistivities themselves might not change too much, the related susceptibilities [involving division by the small resistivity as in Eq. (1)] could be more sensitive.

Our results exhibit in considerable detail the theoretically expected strain dependence of resistivity and LDOS as well as optical weight. The derived susceptibilities depend sensitively on the magnitude and sign of t' . Our results in Fig. (2) and Fig. (3) illustrate the quantitative change of the strain dependence due to varying the magnitude and sign of t' . We should stress that the absolute scale of t is important in determining the T dependence. For illustration we have used $t = 0.45\text{eV}$ in the present paper while the more fine-tuned estimates in [6] suggest a material dependent and somewhat larger value of $t \sim 1\text{eV}$ in most cases.

Our results can be converted to actual strains as in Eq. (42), with α in the range $\alpha \in \{2, 5\}$. If data is available one may ideally eliminate α by measuring the strain dependence of the LDOS or the optical conductivity sum-rule.

B. Comments on experiments

The results found in Fig. 2 yield a magnitude of the nematic susceptibility $\chi_{nem} \sim (1-5)\alpha$ for cuprates. Using the expected range of $\alpha \in \{2, 5\}$, we find $\chi_{nem} \sim (2-25)$. On the other hand, iron based pnictide superconductors appear to have a considerably larger value for χ_{nem} , e.g., in Fig. (3) of Ref. [1] the range $|\chi_{nem}| \lesssim 650$ is reported, thus an order of magnitude greater than our theoretical estimate for cuprates. While fluctuations may drive the magnitude of nematicity further upwards, especially at some densities and temperatures, it appears that the baseline magnitude of this object is itself much larger than expected in cuprates. For example in the four featureless curves of Fig. (3) of Ref. [1] we see that $|\chi_{nem}| \sim 200$.

This magnitude indicates that the downfolding of the many bands of the pnictides to an effective single (or few) band model must yield hopping parameters that are

much more sensitive to strain than in cuprates. The different type of quantum overlap of relevant atomic orbitals from those in cuprates are presumably the origin of this difference. We also note that the sharp peaks in $|\chi_{nem}|$ on varying T , as reported in [1,3] are missing in our results. Instead we have a monotonic increase of $|\chi_{nem}|$ and related susceptibilities as we cool the system, as seen in Fig. 2 and Fig. 4. This increase is largely due to the decrease of the (unstrained) resistivity with lowering T in the Fermi liquid regime.

The sign of χ_{nem} presents a more subtle problem. In iron pnictides it is known to be sensitive to effective mass anisotropy. In fact it changes sign with doping in certain hole-doped iron pnictides [58]. Our single band model lacks such an anisotropy and is therefore not appropriate to describe the elastoresistivity of iron pnictide materials.

After initial submission of our manuscript, we came across the recent measurement of the elastoresistivity nematic susceptibility in Ref. [59] on the two layer cuprate Bi2212. In this experiment, the magnitude of the nematic susceptibility is found to be in the range $|\chi_{nem}| \in \{2.5, 5\}$. This range is consistent with our theoretical estimate. It is also smaller than the nematic susceptibility in iron pnictides by about two orders of magnitude.

The sign of the nematic susceptibility χ_{nem} (Eq. (1)) reported in Ref. [59] implies that the resistivity *increases* in the direction of compression. This result has the opposite sign to our theoretical result as seen in Fig. 2. There we see that the theoretical resistivity *decreases* in the direction of compression, although it does *increase* in the transverse direction. It is possible that the two layer nature of Bi2212 might be responsible for this opposite sign. Also as noted in Fig. 5, the behavior of the nematic susceptibility $\chi_{nem} = \lim_{\epsilon_{xx} \rightarrow 0} (\alpha \chi_{xx})$ at sufficiently low T has the potential for a change of sign, depending on how we choose a sufficiently small $|\epsilon_{xx}|$ or $|\delta t/t|$ for the purpose of taking the limit $\lim_{\epsilon_{xx} \rightarrow 0}$. On the experimental side, a more detailed T variation and examining the various susceptibilities listed in Fig. 5 should yield a more complete picture.

The results found here should also motivate further studies of the strain variation of the 3-dimensional electronic bands of cuprates, towards computing strain variation of the resulting 2-dimensional bands found from projecting to a t - t' - J model. These would test the simple assumptions made here between strain and hopping parameters of a reduced 2-dimensional model as presented in Eqs. (22), (27), (28), and (29). It is also possible that under certain situations, the sign of α can even be changed, as a naive interpretation of the experiments of Ref. [59] suggests.

We believe that it is important to study more extensive set of samples including single layer cuprates at various compositions in future. It would also be useful to study the variations of resistivity along different axes, parallel *and* transverse to the strain axis and extend the studies to various T 's. This type of measurements would enable the construction of the symmetry adapted susceptibilities as in Fig. 5, which provide a greater insight in to the results. It would also be of considerable interest to measure the variations of the LDOS and optical weight with strain, as emphasized above.

V. ACKNOWLEDGEMENT:

We thank Professors I. R. Fisher and S. A. Kivelson for stimulating our interest in this problem, and for helpful discussions. We thank Professor T. Shibauchi for helpful explanation of features of Ref. [59]. The work at UCSC was supported by the US Department of Energy (DOE), Office of Science, Basic Energy Sciences (BES), under Award No. DE-FG02-06ER46319. The computation was done on the comet in XSEDE [57] (TG-DMR170044) supported by National Science Foundation grant number ACI-1053575.

¹ J. H. Chu, H. Kuo, J. G. Analytis, I. R. Fisher, Science **337**, 710 (2012).

² M. C. Shapiro, P. Hlobil, A. T. Hristov, A. V. Maharaj, and I. R. Fisher, Phys. Rev. B **92**, 235147 (2015)

³ J. H. Chu, H. Kuo, J. C. Palmstrom, S. A. Kivelson and I. R. Fisher, Science **352**, 958 (2016).

⁴ B.S. Shastry, Phys. Rev. Lett. **107**, 056403 (2011) <http://physics.ucsc.edu/~sriram/papers/ECFL-Reprint-Collection.pdf>

⁵ In the t - t' - J model the first and last term of Eq. 2, referred to as the hopping H_t and exchange H_J term respectively, explicitly expanded as sum over neighbors is

$$H_t + \mu \hat{N} = -t \sum_{\langle ij \rangle \sigma} \tilde{C}_{i\sigma}^\dagger \tilde{C}_{j\sigma} - t' \sum_{\langle\langle ij \rangle\rangle \sigma} \tilde{C}_{i\sigma}^\dagger \tilde{C}_{j\sigma},$$

$$H_J = \frac{J}{2} \sum_{\langle ij \rangle} \left(\vec{S}_i \cdot \vec{S}_j - \frac{1}{4} n_i n_j \right),$$

where $\langle ij \rangle$ is the sum over nearest neighbors, and $\langle\langle ij \rangle\rangle$ is the sum over second nearest neighbors. In terms of the Hubbard operators — see Eq. (4)—this becomes

$$H_t + \mu \sum_{i\sigma} X_i^{\sigma\sigma} = -t \sum_{\langle ij \rangle \sigma} X_i^{\sigma 0} X_j^{0\sigma} - t' \sum_{\langle\langle ij \rangle\rangle \sigma} X_i^{\sigma 0} X_j^{0\sigma},$$

$$H_J = \frac{J}{2} \sum_{\langle ij \rangle \sigma} X_i^{\sigma\sigma} + \frac{J}{4} \sum_{\langle ij \rangle \sigma_1 \sigma_2} \{ X_i^{\sigma_1 \sigma_2} X_j^{\sigma_2 \sigma_1} - X_i^{\sigma_1 \sigma_1} X_j^{\sigma_2 \sigma_2} \}.$$

- ⁶ B. S. Shastry and P. Mai [arXiv:1911.09119](#).
- ⁷ B. S. Shastry and P. Mai, New J. Phys. **20** 013027 (2018)
- ⁸ P. Mai and B. S. Shastry Phys. Rev. B **98**, 205106 (2018)
- ⁹ F. C. Zhang and T. M. Rice, Phys. Rev. B **41**, 7243 (1990);
- ¹⁰ B. S. Shastry, Phys. Rev. Letts. **63**, 1288 (1989).
- ¹¹ R. S. Markiewicz,¹ S. Sahrakorpi,¹ M. Lindroos,^{1,2} Hsin Lin,¹ and A. Bansil, Phys. Rev. B **72**, 054519 (2005).
- ¹² V. Heine, Phys. Rev. **153**, p. 673 (1967).
- ¹³ Y. Onose, Y. Taguchi, K. Ishizaka, and Y. Tokura, Phys. Rev. B **69**, 024504 (2004).
- ¹⁴ R. L. Greene, P. R. Mandal, N. R. Poniatowski and T. Sarkar, [arXiv:1905.04998](#) (2019).
- ¹⁵ Y. Ando, S. Komiya, K. Segawa, S. Ono, and Y. Kurita, Phys. Rev. Lett. **93**, 267001 (2004).
- ¹⁶ A. Georges, G. Kotliar, W. Krauth, and M. J. Rozenberg, Rev. Mod. Phys. **68**, 13 (1996)
- ¹⁷ G. Kotliar, S. Y. Savrasov, K. Haule, V. S. Oudovenko, O. Parcollet and C. A. Marianetti, Rev. Mod. Phys. **78** 865 (2006).
- ¹⁸ W. Xu, K. Haule, and G. Kotliar, Phys. Rev. Lett. **111**, 036401 (2013).
- ¹⁹ X.Y. Deng, J. Mravlje, R. Žitko, M. Ferrero, G. Kotliar and A. Georges, Phys. Rev. Lett. **110**, 086401 (2013).
- ²⁰ K. Bouadim, N. Paris, F. Hebert, G. G. Batrouni, and R. T. Scalettar, Phys. Rev. B **76**, 085112 (2007).
- ²¹ E. W. Huang, R. Sheppard, B. Moritz and T. P. Devereaux, [arXiv:1806.08346v2](#) (2019).
- ²² T. A. Maier, M. Jarrell, T. Prushke, and M. H. Hettler, Rev. Mod. Phys. **77**, 1027 (2005).
- ²³ Y. Zhang, Y. F. Zhang, S. X. Yang, K.-M. Tam, N. S. Vidhyadhiraja and M. Jarrell Phys. Rev. B **95** 144208 (2017).
- ²⁴ B. S. Shastry, Phys. Rev. B **87**, 125124 (2013)
- ²⁵ B. S. Shastry and E. Perepelitsky, [arXiv:1605.08213](#). Phys. Rev. B **94**, 045138 (2016); R. Žitko, D. Hansen, E. Perepelitsky, J. Mravlje, A. Georges and B. S. Shastry, [arXiv:1309.5284](#) (2013), Phys. Rev. B **88**, 235132 (2013); B. S. Shastry, E. Perepelitsky and A. C. Hewson, [arXiv:1307.3492](#), Phys. Rev. B **88**, 205108 (2013).
- ²⁶ A. Damascelli, Z. Hussain, and Z.-X. Shen, Rev. Mod. Phys. **75**, 473 (2003).
- ²⁷ W. S. Lee, I. M. Vishik, D. H. Lu and Z.-X. Shen, J. Phys.: Condens. Matter **21**, 164217 (2009).
- ²⁸ J. D. Koralek, J. F. Douglas, N. C. Plumb, Z. Sun, A. V. Federov, M. M. Murnane, H. C. Kapteyn, S. T. Cundiff, Y. Aiura, K. Oka, H. Eisaki, and D. S. Dessau, Phys. Rev. Lett. **96**, 017005 (2006).
- ²⁹ T. Yoshida, X. J. Zhou, D. H. Lu, S. Komiya, Y. Ando, H. Eisaki, T. Kakeshita, S. Uchida, Z. Hussain, Z.-X. Shen and A. Fujimori, J. Phys.: Condens. Matter **19** 125209 (2007).
- ³⁰ N. P. Armitage, D. H. Lu, C. Kim, A. Damascelli, K. M. Shen, F. Ronning, D. L. Feng, P. Bogdanov, X. J. Zhou, W. L. Yang, Z. Hussain, P. K. Mang, N. Kaneko, M. Greven, Y. Onose, Y. Taguchi, Y. Tokura, and Z.-X. Shen, Phys. Rev. B **68** 064517 (2003).
- ³¹ G. -H. Gweon, B. S. Shastry, and G. D. Gu, Phys. Rev. Lett. **107**, 056404 (2011).
- ³² P. Mai and B. S. Shastry, Phys. Rev. B **98**, 115101 (2018).
- ³³ A. Koitzsch, G. Blumberg, A. Gozar, B. S. Dennis, P. Fournier, and R. L. Greene, Phys. Rev. B **67** 184522 (2003).
- ³⁴ W. Ding, R. Žitko, P. Mai, E. Perepelitsky and B. S. Shastry, [arXiv:1703.02206v2](#), Phys. Rev. B **96**, 054114 (2017); W. Ding, R. Žitko, and B. S. Shastry, Phys. Rev. B **96**, 115153 (2017).
- ³⁵ This can be seen e.g. Eq. (11), where the “interaction” term in the self-energy is determined by the $\varepsilon_{\vec{k}}$ ’s, the Fourier transform of the hopping matrix elements.
- ³⁶ D. N. Basov and T. Timusk, Rev. Mod. Phys. **77**, 721 (2005).
- ³⁷ D. N. Basov, R. D. Averitt, D. van der Marel, M. Dressel, and K. Haule, Rev. Mod. Phys. **83**, 471 (2011).
- ³⁸ F. Ming, S. Johnston, D. Mulugeta, T. S. Smith, P. Vilmercati, G. Lee, T. A. Maier, P. C. Snijders, and H. H. Weiering, Phys. Rev. Lett. **119**, 266802 (2017).
- ³⁹ Y. J. Yan, M. Q. Ren, H. C. Xu, B. P. Xie, R. Tao, H. Y. Choi, N. Lee, Y. J. Choi, T. Zhang, and D. L. Feng, Phys. Rev. X **5**, 041018 (2015).
- ⁴⁰ P. Choubey, A. Kreisel, T. Berlijn, B. M. Andersen, and P. J. Hirschfeld, Phys. Rev. B **96**, 174523 (2017).
- ⁴¹ A. Kreisel, P. Choubey, T. Berlijn, W. Ku, B. M. Andersen, and P. J. Hirschfeld, Phys. Rev. Lett. **114**, 217002 (2015).
- ⁴² K. Fujita, A. R. Schmidt, E. -A. Kim, M. J. Lawler, D. H. Lee, J. C. Davis, H. Eisaki, and S. -i. Uchida, J. Phys. Soc. Jpn. **81**, 011005 (2012).
- ⁴³ P. W. Anderson, Science **235**, 1196 (1987).
- ⁴⁴ L. P. Kadanoff, G. Baym, Quantum Statistical Mechanics: Green’s Function Methods in Equilibrium and Nonequilibrium Problem, Benjamin, NY, 1962
- ⁴⁵ T. Arai and M. H. Cohen, Phys. Rev. B **21**, 3300 (1980); Phys. Rev. B **21**, 3309 (1980); T. Arai, Phys. Rev. B **21**, 3320 (1980)
- ⁴⁶ P. Mai, S. R. White and B. S. Shastry, Phys. Rev. B **98**, 035108 (2018).
- ⁴⁷ Here $J_{\vec{q}}$ is the Fourier transform of J_{ij} over nearest neighbors. For a homogeneous and translationally invariant system, the Fourier transform gives $J_{\vec{q}} = 2J_x \cos(q_x a) + 2J_y \cos(q_y b)$ on a rectangular lattice where J_x and J_y are the exchange parameter along the principle axes.
- ⁴⁸ M. Ogata and H. Fukuyama *Rep. Prog. Phys.* **71**, 036501 (2008).
- ⁴⁹ We refer to $n = 0.85$ as the optimal density since in a typical single-layer cuprate superconductors such as $\text{La}_{2-x}\text{Sr}_x\text{CuO}_4$ (LSCO) — to which the 2D t - J model is most relevant the system — obtains its maximum critical temperature T_c at hole doping $\delta = 0.15$. Similarly, $\text{Ba}_2\text{Sr}_2\text{CaCu}_2\text{O}_{8+\delta}$ (Bi2212) a double-layer cuprate superconductor obtains its max T_c at doping $\delta = 0.15$.
- ⁵⁰ M. Tinkham, *Group Theory and Quantum Mechanics* (McGraw-Hill, 1964)
- ⁵¹ M. Hamermesh, *Group Theory And Its Application To Physical Problems* (Addison-Wesley Pub. Co., 1962)
- ⁵² L. D. Landau, & E. M. Lifshitz, Vol. 3. *Quantum Mechanics: Non-Relativistic Theory*, 3rd edition, (Elsevier, 1991), p. 366
- ⁵³ The unstrained system assumes a body-centered orthorhombic unit cell (a, b, c) where a, b are the lattice constants of the base and c is that of the height. In the expression for resistivity ρ_0, ϵ_0 corresponds to the interlayer separation $\epsilon_0 = c/2$ between copper-oxide planes.
- ⁵⁴ Y. Ando, in *High T_c Superconductors and Related Transition Metal Oxides* (A Bussmann-Holder and H Keller, Springer, Berlin, 2007) pp. 17-28
- ⁵⁵ See Supplemental Material at [URL will be inserted by publisher] for further discussion and supplemental figures on the effects of an x-axis strain on the resistivity, kinetic energy and local density of states.
- ⁵⁶ In high T_c systems estimates give $t' \lesssim -0.27t$ Bi2212 and LSCO $t' \sim 0.16t$. We take $t' = -0.2t$ as a compromise between the two extremes.

- ⁵⁷ J. Town et al., “XSEDE: Accelerating Scientific Discovery”, *Computing in Science & Engineering*, Vol.16, No. 5, pp. 62-74, Sept.-Oct. 2014, doi:10.1109/MCSE.2014.80
- ⁵⁸ E. C. Blomberg, M. A. Tanatar, R. M. Fernandes, I. I. Mazin, Bing Shen, Hai-Hu Wen, M. D. Johannes, J. Schmalian and R. Prozorov, *Nature Communications* **4** 1914 (2013)
- ⁵⁹ K. Ishida, S. Hosoi, Y. Teramoto, T. Usui, Y. Mizukami, K. Itaka, Y. Matsuda, T. Watanabe, and T. Shibauchi, [arXiv:1908.07167](#).

Supplementary Material: Theory of anisotropic elastoresistivity of two-dimensional extremely strongly correlated metals

Michael Arciniaga¹, Peizhi Mai^{2,1}, B Sriram Shastry¹

¹*Physics Department, University of California, Santa Cruz, CA 95064, USA and*

²*Center for Nanophase Materials Sciences, Oak Ridge National Laboratory, Oak Ridge, TN, 37831-6494, USA*

(Dated: November 12, 2021)

I. OVERVIEW

The Supplementary Material (SM) sections are organized as follows: In Sec. II we expand the resistivity analysis by discussing the role of different terms on the resistivity calculation under an x-axis strain. In Sec. III we examine the effects of strain on the total kinetic energy and the longitudinal and transverse susceptibilities over a broad temperature range. In Sec. IV we present supplemental figures showing the effects of strain on the local density of states (LDOS) in different materials for both non-interacting (bare band structure) and interacting (t - t' - J model) systems.

II. RESISTIVITY FOR AN X-AXIS STRAIN : ROLE OF DIFFERENT FACTORS

Here we further explore the effects of strain on electrical resistivity and their associated susceptibilities in response to an x-axis strain for an extremely correlated Fermi liquid [S1,S2] (ECFL). In order to gauge the relative importance of strain in the resistivity calculation [S3], it is useful to study the effect of strain on each term in conductivity calculation:

$$\sigma_{xx} = \left\langle \Upsilon_{\vec{k}} \left(\frac{\partial \epsilon_{\vec{k}}}{\partial k_1} \right)^2 (a/b) \right\rangle_k, \quad (\text{S1})$$

$$\sigma_{yy} = \left\langle \Upsilon_{\vec{k}} \left(\frac{\partial \epsilon_{\vec{k}}}{\partial k_2} \right)^2 (b/a) \right\rangle_k. \quad (\text{S2})$$

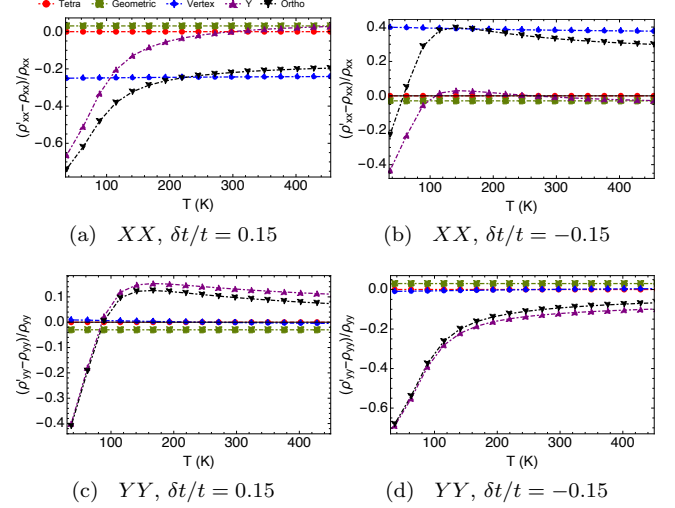
Furthermore we note that strain affects conductivity in two fashions: it produces a change (1) in the lattice constant

$$a \rightarrow a_0 + \delta a; \quad b \rightarrow a_0; \quad \rho \rightarrow \sqrt{2}a_0 + \frac{\delta a}{\sqrt{2}}, \quad (\text{S3})$$

and (2) in the hopping parameters

$$t_x = (1 - \alpha \epsilon_{xx}) t; \quad t_y = t; \quad t_d = \left(1 - \alpha \frac{\epsilon_{xx}}{2} \right) t'. \quad (\text{S4})$$

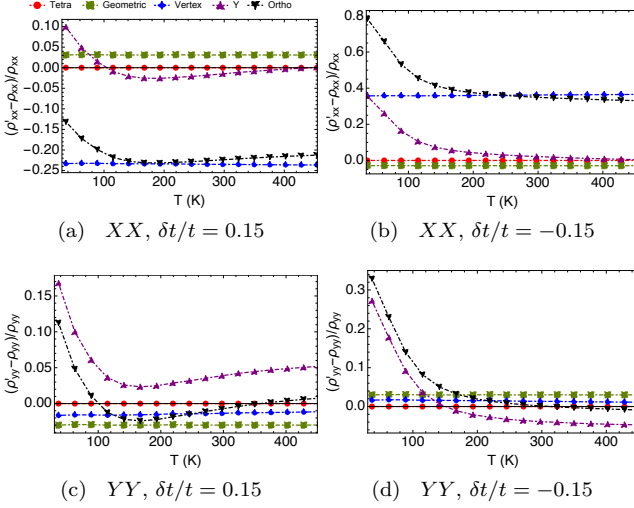
The distorted lattice constants play the role of a dimensionless coefficient in Eqs. (S1) and (S2). The modified hopping parameters comes into play through the bare vertices and the spectral function in $\Upsilon_{\vec{k}}$ (see Eq. 34 of



S-FIG. 1: The normalized resistivity response vs T isolating the effects of different terms in Eqs. (S1) and (S2) for a hole doped material. The curve labeled “Geometric” gauges the sensitivity of resistivity to a direct change in lattice parameters a and b . “Vertex” examines the effects of strain on $\partial \epsilon_{\vec{k}} / \partial k_i$ which is modified to be only a function of t, t' . “Y” isolates the effects of strain on ρg . “Tetra” is the unstrained resistivity while “Ortho” includes the strain-induced effects from all the terms. All figures share a legend. The parameters set is filling $n = 0.85$, $t' = -0.2t$ and strain of magnitude $|\delta t/t| = 0.15$.

the main text). Specifically, we compute the conductivity while isolating the effects of strain to the following terms: (1) the spectral functions in $\Upsilon_{\vec{k}}$, (2) the “vertex” $\partial \epsilon_{\vec{k}} / \partial k_i$ for $i = 1, 2$, and (3) the distorted lattice constants a, b , denoted “Geometric” which separates out the strain-induced effects on the correlations, band structure and geometry, respectively, and we record the sensitivity of conductivity to each term.

In S-Fig. 1 we gauge the sensitivity of different terms in Eqs. (S1) and (S2) to the effects of strain on the normalized longitudinal and transverse resistivity response as a function of temperature for a hole-doped material at optimal density for both a compressive and tensile strain. Additionally we show for comparison the resistivity calculation on the unstrained tetragonal lattice denoted “Tetra” and we show a calculation of the resistivity response on the strain-induced orthorhombic lattice called “Ortho”. The latter curve combines the effects of

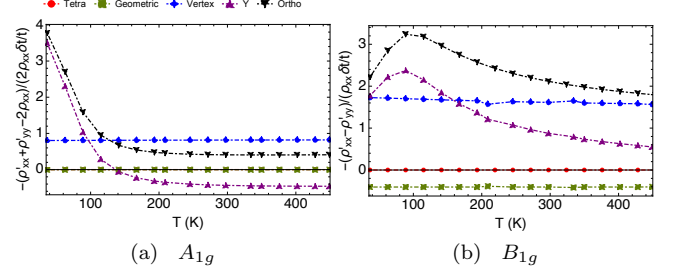


S-FIG. 2: The effects of strain on the normalized resistivity response vs T isolating different terms in Eqs. (S1) and (S2) for an electron-doped material. The parameter set is $n = 0.85$, $t' = 0.2t$ and a strain of magnitude $|\delta t/t| = 0.15$. (a)-(b) longitudinal response; (c)-(d) transverse response. All figures share a legend.

strain from each term. We note that the strain-induced effects from the change in the lattice constant is small compared to the other terms. We observe that the longitudinal resistivity strain response is dominated by the vertex contribution at high temperature, while the effect of $\Upsilon_{\vec{k}}$ becomes more and more important in modifying the T -dependent behavior of the longitudinal response when decreasing the temperature, as seen in panels (a) and (b). The transverse resistivity, shown in panels (c) and (d), is mostly sensitive to the effect of strain on the spectral functions, i.e., $\Upsilon_{\vec{k}}$ and therefore the interactions are the dominate source of the response over the entire temperature range.

Now switching gears we examine the strain-induced effects on materials with electron doping, as shown in S-Fig. 2 with parameters set to density $n = 0.85$, second neighbor hopping $t' = 0.2t$, and a strain of magnitude $|\delta t/t| = 0.15$. In the electron-doped case we likewise find that the vertex term enhances the longitudinal resistivity for compressive strain as shown in panel (a) whereas a tensile strain has the opposite effect. On the other hand, we now find that the strain-induced effects contained in $\Upsilon_{\vec{k}}$ term enhances the resistivity at low- T rather than suppressing the resistivity as seen in the hole-doped case. Continuing with the similarities we find that the effects of strain on transverse response from vertex part remains negligible as seen in panels (c)-(d) and therefore the strain-induced effects due to interactions dominate the resistivity calculation. Moreover, we observe a switch in the sign of the response as we move from hole-doped to electron-doped which follows from the dominance of the strain-induced effects on the correlations.

In Figure 3 we have the response function for the irrep



S-FIG. 3: The strain-induced resistivity response vs T for (a) A_{1g} and (b) B_{1g} irreps, isolating different terms in Eqs. (S1) and (S2), for a material with hole doping. The parameter set is $n = 0.85$, $t' = -0.2t$, with a compressive strain $\delta t/t = -0.15$. All figures share a legend.

A_{1g} and B_{1g} , respectively [S4]. As one might expect, these curves are sensitive to both the vertex part and the spectral function. We also note that the source of the T -dependence is the spectral function and that the dominate source of asymmetry between compressive and tensile strains for the A_{1g} and B_{1g} irreps is the vertex part at high- T and the $\Upsilon_{\vec{k}}$ term at low- T .

III. KINETIC ENERGY

A. The raw kinetic energies

S-Fig. 4 shows the total kinetic energy K_{tot} versus T at various t' and $\delta t/t$. The total kinetic energy for a system under strain is computed as

$$K_{\text{tot}} = \left\langle \int_{-\infty}^{\infty} \rho g(k) \epsilon_{\vec{k}} d\omega \right\rangle_k. \quad (\text{S5})$$

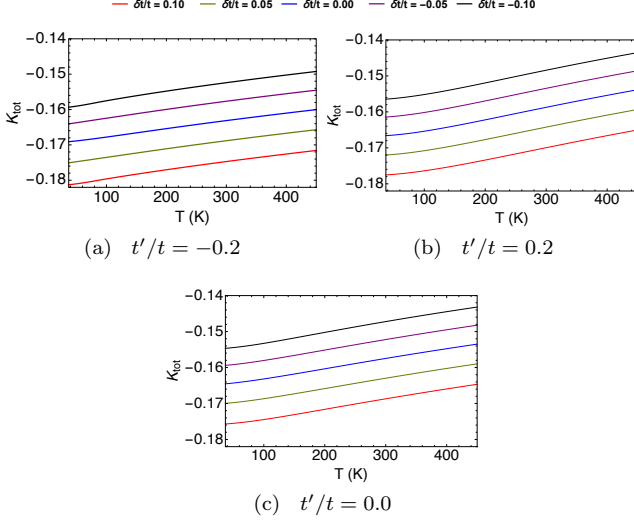
We observe that decreasing the strain at a fixed T increases the total kinetic energy for all t' which indicates that the scale of the optical conductivity increases as the strain gets weaker. Recall that in the t - t' - J model the kinetic energy is related to optical conductivity through the f-sum rule [S5,S6] (see Eq. (53) of the main text). We also note that the curvature of the line shape, similar to ρ - T curves, slightly changes from negative to positive as t' increases from negative (hole-like) to positive (electron-like).

B. The longitudinal and transverse susceptibilities

The strain-kinetic-energy susceptibility for the longitudinal and transverse directions are defined in terms of hopping strain as

$$M_{XX} \equiv -\left(\frac{K'_{xx} - K_{xx}}{K_{xx}} \right) / \left(\frac{\delta t}{t} \right), \quad (\text{S6})$$

$$M_{YY} \equiv -\left(\frac{K'_{yy} - K_{yy}}{K_{xx}} \right) / \left(\frac{\delta t}{t} \right), \quad (\text{S7})$$



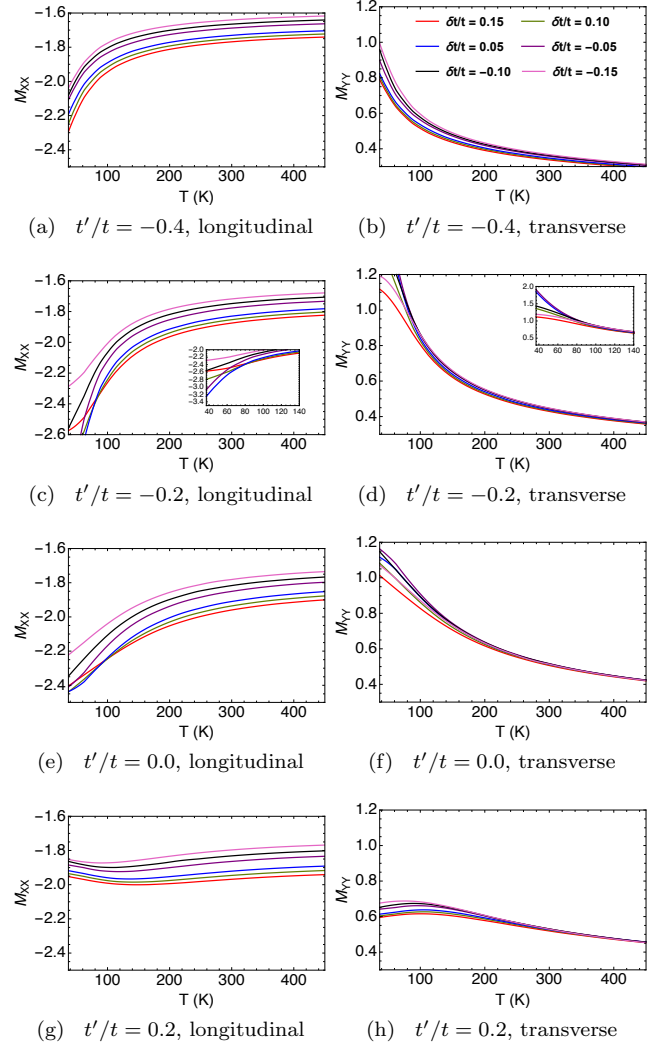
S-FIG. 4: The total kinetic energy at optimal filling $n = 0.85$, at various t' , for various $\delta t/t$. All figures shared a legend.

respectively. We plot the longitudinal and transverse strain-kinetic-energy susceptibilities versus temperature as shown in S-Fig. 5 for the optimal doping ($n = 0.85$) case at various t' and $\delta t/t$. Similar to the results for the resistivity response functions we find that the transverse response functions are nearly linear at high- T whereas the longitudinal response functions are non-linear throughout the temperature range and as expected the intensity of the transverse response function is weaker in comparison to the longitudinal.

Finally, looking at the strain dependence we find that the susceptibilities increase monotonically as strain is varied from compressive to tensile for nearly all t' with notable exception of $t' = -0.2t$ (approximately the parameter for LSCO) which at low- T the response function increases monotonically with the intensity of the strain with a slight asymmetry between tensile and compressive strains. For all other t' we see, e.g. in S-Fig. 5 (f), that the transverse kinetic energy cannot resolve between different tensile strains ($\delta t/t < 0.0$) until very low temperatures whereas it is quite distinguishable for the longitudinal case and likewise for the compressive strains.

IV. THE LOCAL DENSITY OF STATES : STRAIN VARIATION

In S-Figs. 6, we present the LDOS at optimal density ($n = 0.85$) at $T = 37\text{K}$ and room temperature ($T = 298\text{K}$) for various t' and $\delta t/t$ for systems with and without interactions. In panels (a)-(d) we have the bare LDOS where we find that strain causes a highly localized inversion of the peak, resulting in a valley centered at same approximate position along the spectrum. The valley is surrounded by a peak on each side at a reduced height and the weight of spectrum is lifted to the back-

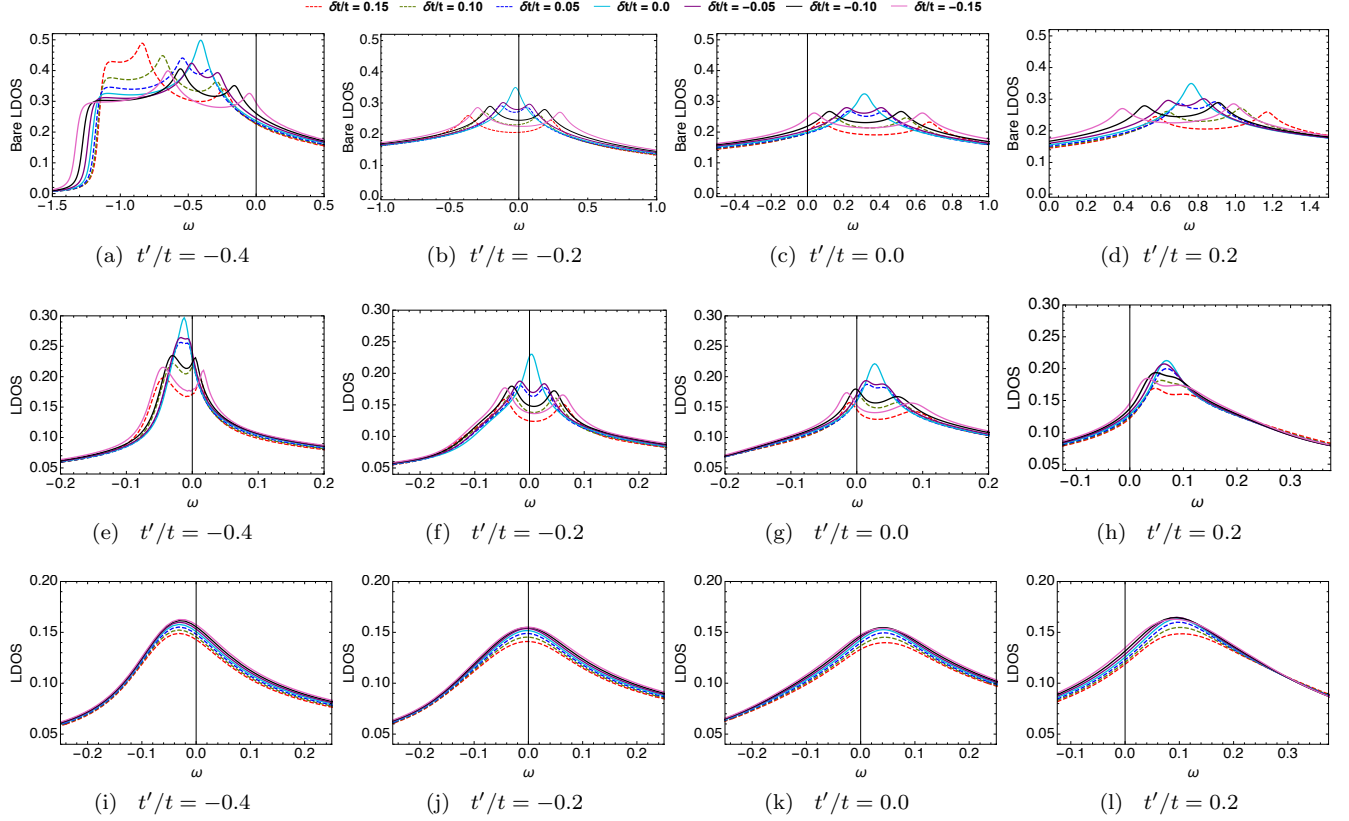


S-FIG. 5: The normalized strain-kinetic-energy susceptibilities for longitudinal and transverse components from Eq. (S6) and Eq. (S7), respectively, at optimal doping $n = 0.85$, for various t' and $\delta t/t$. All figures share a legend.

ground.

For $t'/t < 0$ ($t'/t > 0$) the bare LDOS peak heights are asymmetric, higher on the left (right), and shifted left (right) on the spectrum, whereas for $t'/t = 0$ the LDOS peaks are symmetric. We also notice an asymmetry between a compressive strain ($\delta t/t > 0$) and a tensile strain ($\delta t/t < 0$) where the bare LDOS peak heights are more strongly inverted for the former except for $t'/t = -0.4$ since it is constrained by the band edge.

We see that at low temperatures, i.e. $T = 37\text{K}$ as seen in panels (e)-(h), the double peak persists for all strains, however, the peaks remain asymmetric favoring the left hand side for all t' . In previous work [S7], it was shown that systems with high t' have higher Fermi liquid temperature scales, making them more robust to warming, that is, the LDOS peaks will have a slower rate of change (smoothing and broadening) in response to warming.



S-FIG. 6: The local density of states versus frequency at optimal filling $n = 0.85$, at $T = 37\text{K}$ and room temperature ($T = 298\text{K}$), for various $t' = -0.4, -0.2, 0.0, 0.2$ at select $\delta t/t$. (a)-(d) The non-interacting system (i.e., band structure), $T = 298\text{K}$; (e)-(h) the interacting system, $T = 37\text{K}$; (i)-(l) the interacting system, $T = 298\text{K}$. All figures share a legend.

Although we may expect the Fermi liquid temperature scale to warm as the hopping strain increases from negative (tensile) to positive (compressive), we find that the scale is similar for compressive and tensile strains of identical magnitude as seen in panels (i)-(l). This is a result of the anisotropy of the resistivity, producing two chan-

nels and hence two Fermi temperature scales. We find that the rate of change in LDOS peaks scales with the average ratio of the hopping parameters $(t_d/t_x + t_d/t_y)/2$, where t_d/t_x and t_d/t_y correspond with the Fermi temperature scale for the longitudinal and transverse resistivity, respectively.

[S1] B. S. Shastry, Phys. Rev. Lett. **107**, 056403 (2011). <http://physics.ucsc.edu/~sriram/papers/ECFL-Reprint-Collection.pdf>
[S2] B. S. Shastry, Phys. Rev. B **87**, 125124 (2013).
[S3] B. S. Shastry and P. Mai, New J. Phys. **20** 013027 (2018).
[S4] M. C. Shapiro, P. Hlobil, A. T. Hristov, A. V. Maharaj, and I. R. Fisher, Phys. Rev. B **92**, 235147 (2015)

[S5] D. N. Basov and T. Timusk, Rev. Mod. Phys. **77**, 721 (2005).
[S6] D. N. Basov, R. D. Averitt, D. van der Marel, M. Dressel, and K. Haule, Rev. Mod. Phys. **83**, 471 (2011)
[S7] P. Mai and B. S. Shastry, Phys. Rev. B **98**, 205106 (2018).